Japanese Journal of Radiology (2022) 40:341–366
https://doi.org/10.1007/s11604-021-01223-4

INVITED REVIEW

Dynamic contrast-enhanced (DCE) imaging: state of the art and applications in whole-body imaging

Domenico Albano[1,2,3] · Federico Bruno[1,4] · Andrea Agostini[1,5] · Salvatore Alessio Angileri[1,6] · Massimo Benenati[1,7] · Giulia Bicchierai[8] · Michaela Cellina[9] · Vito Chianca[10,11] · Diletta Cozzi[1,12] · Ginevra Danti[12] · Federica De Muzio[13] · Letizia Di Meglio[14] · Francesco Gentili[15] · Giuliana Giacobbe[1,16] · Giulia Grazzini[17] · Irene Grazzini[18] · Pasquale Guerriero[1,13] · Carmelo Messina[2] · Giuseppe Micci[1,3] · Pierpaolo Palumbo[1,19] · Maria Paola Rocco[16] · Roberto Grassi[1,16] · Vittorio Miele[1,17] · Antonio Barile[1,4] · on behalf of the Young SIRM Working Group

Received: 6 September 2021 / Accepted: 17 November 2021 / Published online: 24 December 2021

Abstract

Dynamic contrast-enhanced (DCE) imaging is a non-invasive technique used for the evaluation of tissue vascularity features through imaging series acquisition after contrast medium administration. Over the years, the study technique and protocols have evolved, seeing a growing application of this method across different imaging modalities for the study of almost all body districts. The main and most consolidated current applications concern MRI imaging for the study of tumors, but an increasing number of studies are evaluating the use of this technique also for inflammatory pathologies and functional studies. Furthermore, the recent advent of artificial intelligence techniques is opening up a vast scenario for the analysis of quantitative information deriving from DCE. The purpose of this article is to provide a comprehensive update on the techniques, protocols, and clinical applications – both established and emerging – of DCE in whole-body imaging.

Keywords DCE · MRI · Oncology · Radiomics

Domenico Albano and Federico Bruno have Contributed equally.

✉ Federico Bruno
federico.bruno.1988@gmail.com

1 Italian Society of Medical and Interventional Radiology (SIRM), SIRM Foundation, Milan, Italy

2 IRCCS Istituto Ortopedico Galeazzi, Milan, Italy

3 Dipartimento Di Biomedicina, Neuroscienze E Diagnostica Avanzata, Sezione Di Scienze Radiologiche, Università Degli Studi Di Palermo, via Vetoio 1L'Aquila, 67100 Palermo, Italy

4 Department of Biotechnological and Applied Clinical Sciences, University of L'Aquila, L'Aquila, Italy

5 Department of Clinical, Special and Dental Sciences, Department of Radiology, University Politecnica delle Marche, University Hospital "Ospedali Riuniti Umberto I – G.M. Lancisi – G. Salesi", Ancona, Italy

6 Radiology Unit, Fondazione IRCCS Ca' Granda Ospedale Maggiore Policlinico, Milan, Italy

7 Dipartimento di Diagnostica per Immagini, Fondazione Policlinico Universitario A. Gemelli IRCCS, Oncologia ed Ematologia, RadioterapiaRome, Italy

8 Diagnostic Senology Unit, Azienda Ospedaliero-Universitaria Careggi, Florence, Italy

9 Department of Radiology, ASST Fatebenefratelli Sacco, Ospedale Fatebenefratelli, Milan, Italy

10 Ospedale Evangelico Betania, Naples, Italy

11 Clinica Di Radiologia, Istituto Imaging Della Svizzera Italiana - Ente Ospedaliero Cantonale, Lugano, Switzerland

12 Department of Emergency Radiology, Careggi University Hospital, Florence, Italy

13 Department of Medicine and Health Sciences "Vincenzo Tiberio", University of Molise, Campobasso, Italy

14 Postgraduation School in Radiodiagnostics, University of Milan, Milan, Italy

15 Unit of Diagnostic Imaging, Azienda Ospedaliera Universitaria Senese, Siena, Italy

16 Department of Precision Medicine, University of Campania "L. Vanvitelli", Naples, Italy

17 Department of Radiology, Azienda Ospedaliero-Universitaria Careggi, Florence, Italy

18 Department of Radiology, Section of Neuroradiology, San Donato Hospital, Arezzo, Italy

19 Abruzzo Health Unit 1, Department of diagnostic Imaging, Area of Cardiovascular and Interventional Imaging, L'Aquila, Italy

Introduction

Dynamic contrast-enhanced (DCE) imaging is a non-invasive technique used for the evaluation of tissue vascularity features through imaging series acquisition after contrast medium administration [1–4]. Over the years, the study technique and protocols have evolved, seeing a growing application of this method across different imaging modalities for the study of almost all body districts [5–9]. Indeed, with some differences between organs and systems, numerous information can be obtained from the DCE analysis through qualitative, semi-quantitative, and model-based quantitative methods. [10, 11] Qualitative assessment of contrast uptake, wash-in and wash-out rates is the most clinically routinely used method, due to the simple and time-saving visual approach. DCE time–intensity curves can be analyzed semi-quantitatively according to the signal intensity changes to obtain several parameters, such as the time to peak (TTP), wash-in and wash-out rate (WIR/WOR), area under contrast curve (AUC), maximum enhancement (ME), and percent maximum enhancement (%ME) [12, 13] . Full quantitative analysis of the DCE data involves the conversion of signal intensity to gadolinium concentration and fit the data into a tissue model. One of the most used is the Tofts Model, in which each voxel contains tissue cells, blood vessels, and extracellular spaces. According to this model, two main parameters of influx mass transfer rate of gadolinium (Ktrans) from blood plasma to extracellular space, and reflux rate of gadolinium from the extracellular space to blood plasma. (Kep) [14, 15].

The main and most consolidated current applications concern MRI imaging in oncology, but an increasing number of studies are evaluating the use of this technique also for inflammatory pathologies and functional studies [16–21]. Furthermore, the recent advent of artificial intelligence techniques is opening up a vast scenario for the analysis of quantitative information deriving from DCE [22–27]. The purpose of this article is to provide a comprehensive update on the techniques, protocols and clinical applications – both established and emerging – of DCE in whole-body imaging.

Neuroimaging

DCE-MRI is considered the standard approach for assessing brain permeability [28], and has been shown to provide valuable information especially in the evaluation of brain tumors

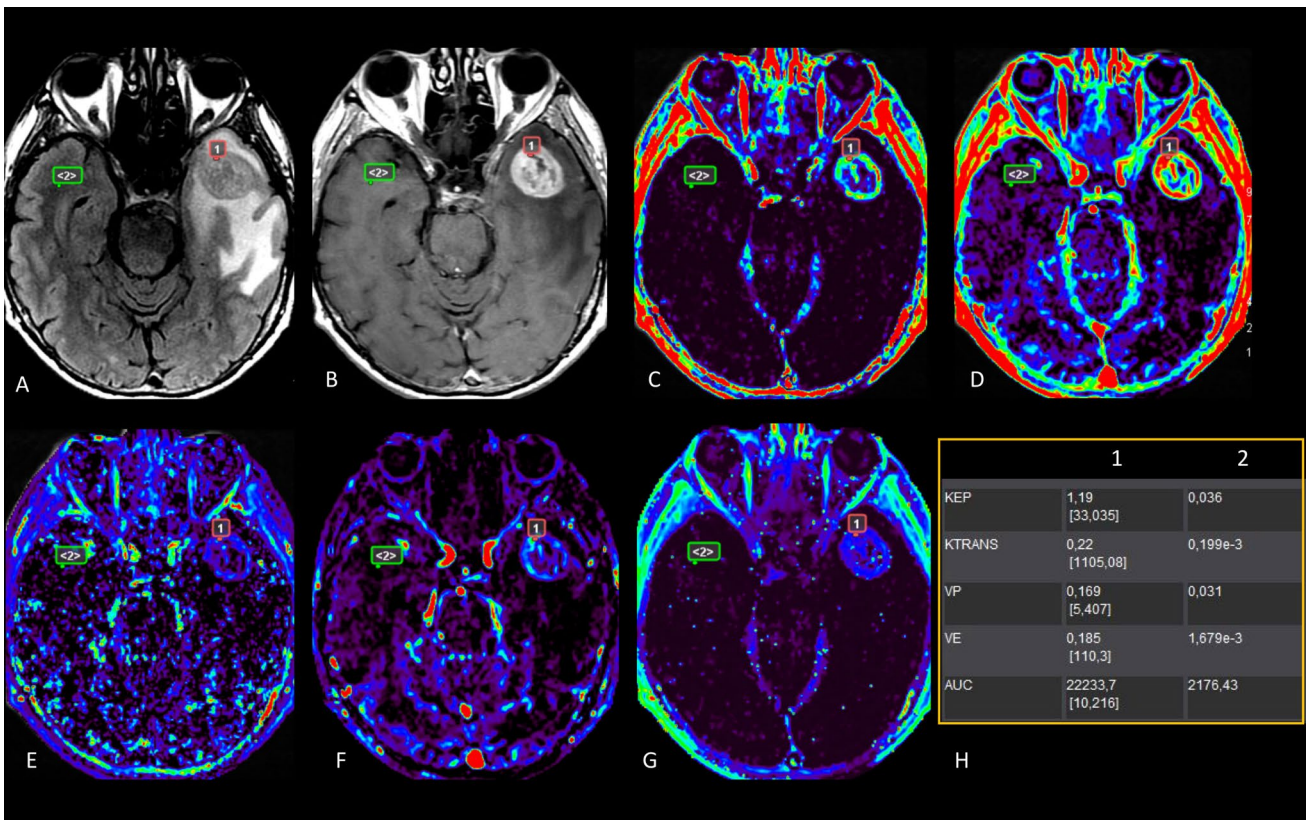

Fig. 1 Glioblastoma WHO IV (high-grade glioma) in a 71-year-old man; morphologic imaging **A** FLAIR and **B** T1+Gd and parametric DCE maps **C** Ktrans, **D** AUC, **E** Kep, **F** Vp, **G** Ve, **H** summary of high perfusion values

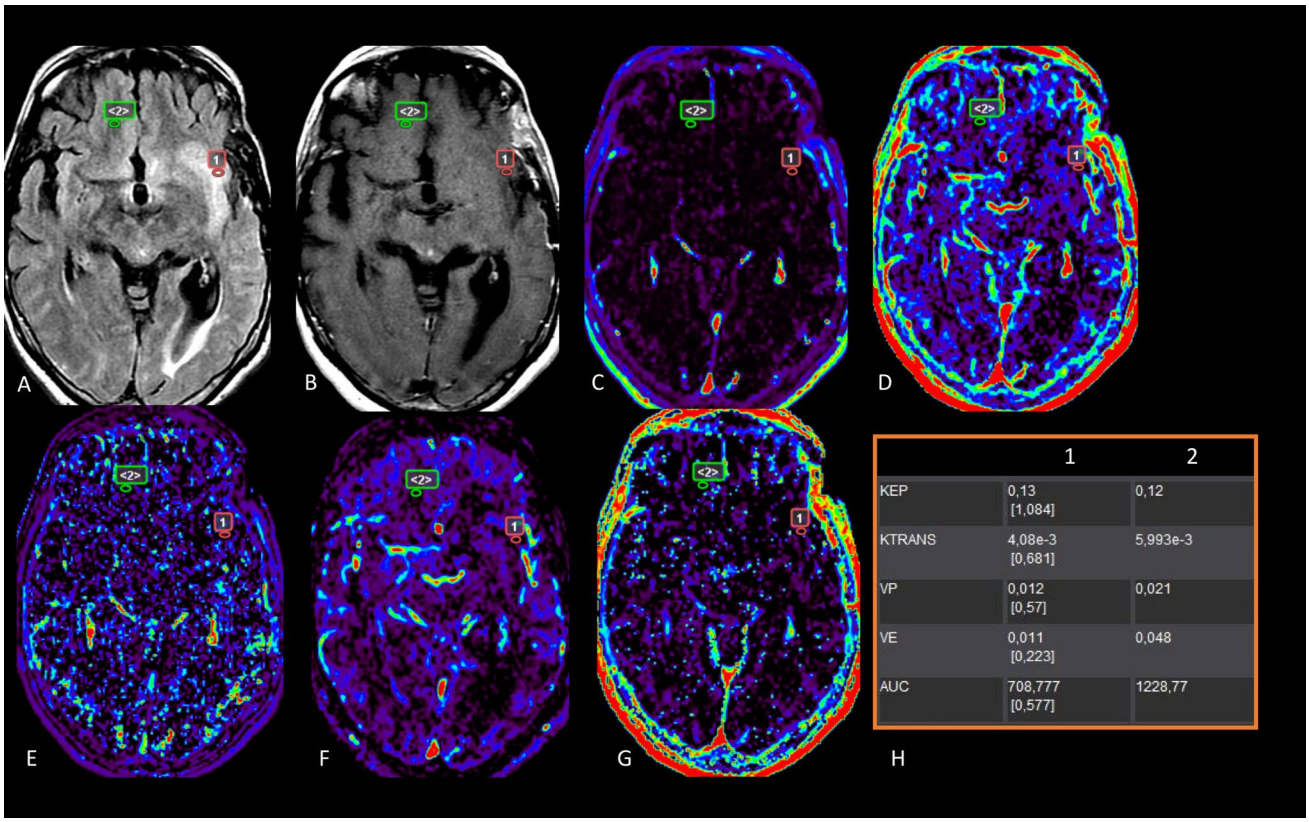

Fig. 2 Diffuse astrocytoma WHO II (low-grade glioma) in a 73-year-old woman; morphologic imaging **A** FLAIR and **B** T1+Gd and parametric DCE maps **C** Ktrans, **D** AUC, **E** Kep, **F** Vp, **G** Ve, and **H** summary of slightly increased perfusion values compared to contralateral normal appearing brain tissue, and lower compared to HGG

[29–32]. Applications of DCE-MRI in gliomas include tumor grading and characterization, treatment response, and prognosis assessment.

Grading

High-grade gliomas (HGG) show higher *K*trans, Ve, and Vp than low-grade gliomas (LGG) [33–37], and Ktrans is considered the most significant parameter for grading [38] (Figs. 1 and 2). Recently, textural features derived from DCE-MRI displayed a good ability in discriminating between different grades of gliomas [39, 40]. The 2016 WHO classification of brain tumors added molecular criteria to histology [41]. Increased *K*trans and *V*p mean/histogram values were observed in EGFRvIII-positive glioblastoma [34]. Ann et al. found that glioblastomas with MGMT methylation had higher *K*trans [42]. Cheng et al reported a positive correlation between Ktrans and VEGF expression in gliomas [43].

Differential diagnosis

Although there is no difference for *K*trans and Vp between glioblastoma and melanoma metastasis, hypovascular metastasis, such as from lung cancer, could be differentiated using Vp, AUC, and logarithmic slope of the wash-out phase [44, 45]. Zhao et al. assessed that Ve in the tumor parenchyma and *K*trans in peritumoral area could discriminate HGG from metastasis [46]. Primary Central Nervous System Lymphoma (PCNSL) demonstrated higher *K*trans, K2, and Ve than glioblastoma and metastases [46–48]. Also, AUC and histogram analysis of DCE identified differences between HGG and PCNSL [49–51]. In addition, pretreatment Vp and Ktrans may be prognostic biomarkers of progression-free survival (PFS) in patients with PCNSL [52], and Ktrans changes were found to predict chemotherapy response [53].

Treatment response assessment

A meta-analysis demonstrated that DCE shows the highest diagnostic accuracy among the perfusion techniques in differentiating between treatment-induced changes and progression [54]. Increased *K*trans has been reported in recurrent lesions in comparison to radionecrosis [55, 56]. *K*trans, Ve, and Vp are higher in progression than in pseudoprogression in patients with glioblastoma, with Ktrans the most promising parameter [57, 58]. Thomas et al. identified a Ktrans threshold of 3.5 for pseudoprogression and of 7.4 for recurrence [58]. Recently, radiomic features obtained from Ktrans achieved a good accuracy in detecting pseudoprogression [59].

Predicting prognosis

Worse survival was reported for glioma patients with high Ktrans and Vp [60]. Kim et al. found higher mean Ve in anaplastic astrocytoma patients with PFS <18 months than that in those with PFS ≥18 months [61]. Beyond neurooncology, DCE has been applied to the assessment of blood brain barrier (BBB) dysfunction in acute ischemic stroke (AIS) and small vessel disease, multiple sclerosis (MS), traumatic brain injury (TBI), migraine, and Alzheimer's Disease (AD) [29, 31]. Stroke Ktrans was described higher compared to mirror Ktrans, and lower than in hemorrhagic transformed regions [62]. DCE-MRA could be used to generate collateral maps in AIS [63]. A recent review showed increased Ktrans and Ve, and decreased Vp following TBI in vulnerable areas, including brain cortex and brainstem [64]. Acute lesions in MS exhibit hyperperfusion [65], while normal-appearing white matter has been found hypoperfused compared with controls [66]. However, the same authors could not confirm these findings in a subsequent paper [67], and the clinical relevance of DCE in MS remains uncertain. Raja et al. reported low permeability in the white matter in AD in comparison to vascular cognitive impairment patients [68]. Global BBB leakage has been associated with cognitive decline in early AD [69]. In migraine patients, the mean Vp in the left amygdala was found lower than that in the healthy controls [70].

Head and neck

Tumor characterization

Primitive H&N cancer has much more responsive microvascular environment than healthy tissue in early acquisition with Ultrafast DCE-MRI [71]. DCE could be crucial, allowing a targeted therapy and improving the prognosis of patients with unknown primary tumors (UPT) and local metastasis by overcoming the limits of DWI (false negative in tonsil tumors) and 18F-FDG-PET/CT (poor anatomical accuracy) [72]. Lee et al observed statistically significant differences of Ktrans value between undifferentiated and HNSCC, and between undifferentiated carcinoma and lymphoma, but no significant differences between HNSCC and lymphoma [3]. Park et al, proved the usefulness of DCE-MRI in the differential diagnosis of HNSCC and oropharyngeal lymphoma, with significantly higher Ktrans values in the first one [73].

Some data are also available on the characterization of the salivary gland lesions (Fig. 3). DCE-MRI generated time/intensity curve with progressive wash-in was observed only in benign lesions, whereas rapid wash-in/slow wash-out associated with ADC 0.9–1.4 × 10−3 mm^2/s showed high specificity for epithelial malignancies [74]. Mungai et al assessed the value of lesion/parenchyma ratio of different DCE-MRI parameters to differentiate benign from malignant lesions and the various types of benign masses [75].

Treatment response prediction and assessment

HNSCC advanced stage can be treated surgically or with chemoradiotherapy, with the latter preferred due to organ integrity preservation. However, 25–30% of HNSCC do not respond to chemoradiotherapy [76]. Pre-treatment DCE-MRI can be used to predict HNSCC response to chemoradiation as an imaging biomarker for hypoxia. Ktrans is the most frequently identified pre-treatment DCE parameter with predictive or prognostic significance, followed by Ve. Further, a high pre-therapy Ktrans level correlated with good treatment response [77]. Lymph nodes DCE-MRI can also be used to predict treatment response. Ng et al reported low pre-treatment lymph node Ve (<0.23) to be an independent poor prognostic factor local control and overall survival [78]. A significant increase of Ktrans and Ve was observed in post-chemoradiation in responder patients [79]. Wang et al proposed identifying neoplasm subvolumes based on heterogeneous distributions of blood volume and blood flow after two weeks of therapy and reported that large poorly perfused subvolumes of cancer and lymph nodes identified at baseline and persisting at an early follow-up, as well as the increase of tumoral subvolumes with low blood flow, can predict local or regional treatment failure [80]. This evidence may be useful in identifying intralesional regions that may benefit from a local dose increase. Post-treatment fibrotic tissue typically exhibits delayed and less avid contrast enhancement, whereas residual/recurrent neoplastic components show earlier and more intense enhancement. Lee et al applied DCE in the detection of local recurrence in HNSCC. They used voxel-based color maps of the AUC values extracted from TSI (time–signal intensity) curves during the initial and final 90 seconds. Recurrent tumors exhibit increased IAUC90 (initial AUC 90-second) values due to neoangiogenesis and contrast agent leakage to the extravascular extracellular space, whereas in post-therapy tissue there is a progressive increase in FAUC90 (final AUC 90-second) due to low cellularity [81].

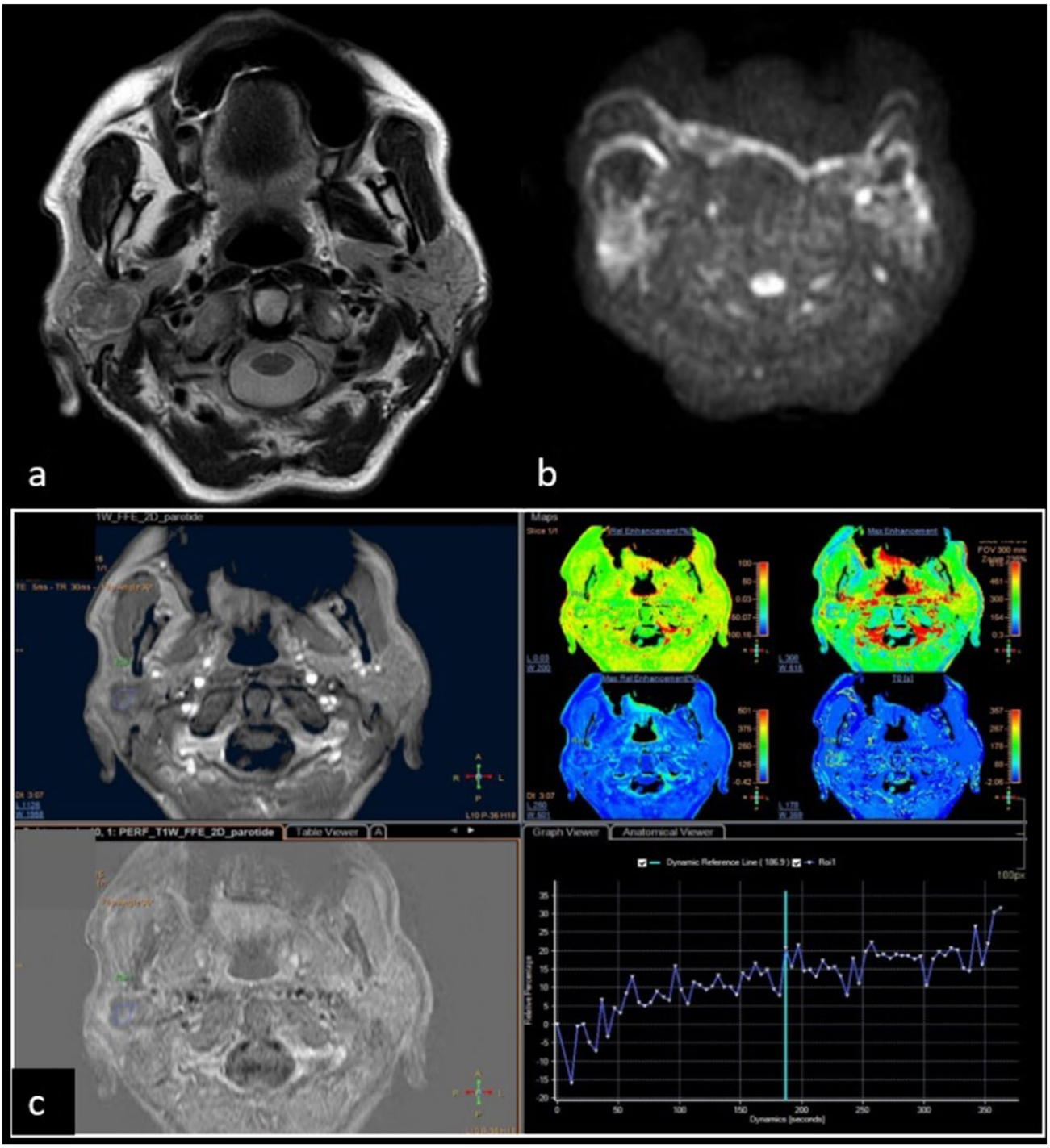

Fig. 3 Pleomorphic adenoma of the right parotid gland in a 56-year-old woman. **a** Axial T2-weighted MR image shows a heterogeneously hypointense mass with a peripheral hyperintense rim in the right parotid gland. **b** ADC map shows a central area of restriction. c the time/intensity curve with the calculation of the maximum contrast enhancement shows a low constant rising, characteristic for benign lesions

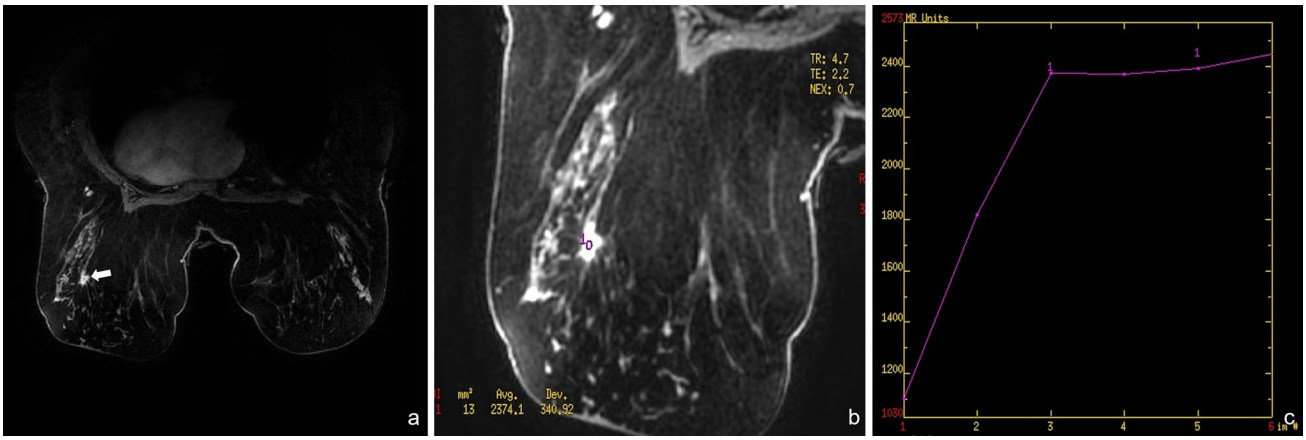

Fig. 4 43-year-old woman. Finding a left-sided parenchymal distortion on a screening examination, without hand-hold ultrasound alterations. **a** DCE image shows a starry lesion in the upper outer quadrant (arrow); **b,c** ROI positioning shows a time–intensity curve type II. Tomosynthesis-guided vacuum-assisted biopsy of this lesion showed ductal carcinoma NOS

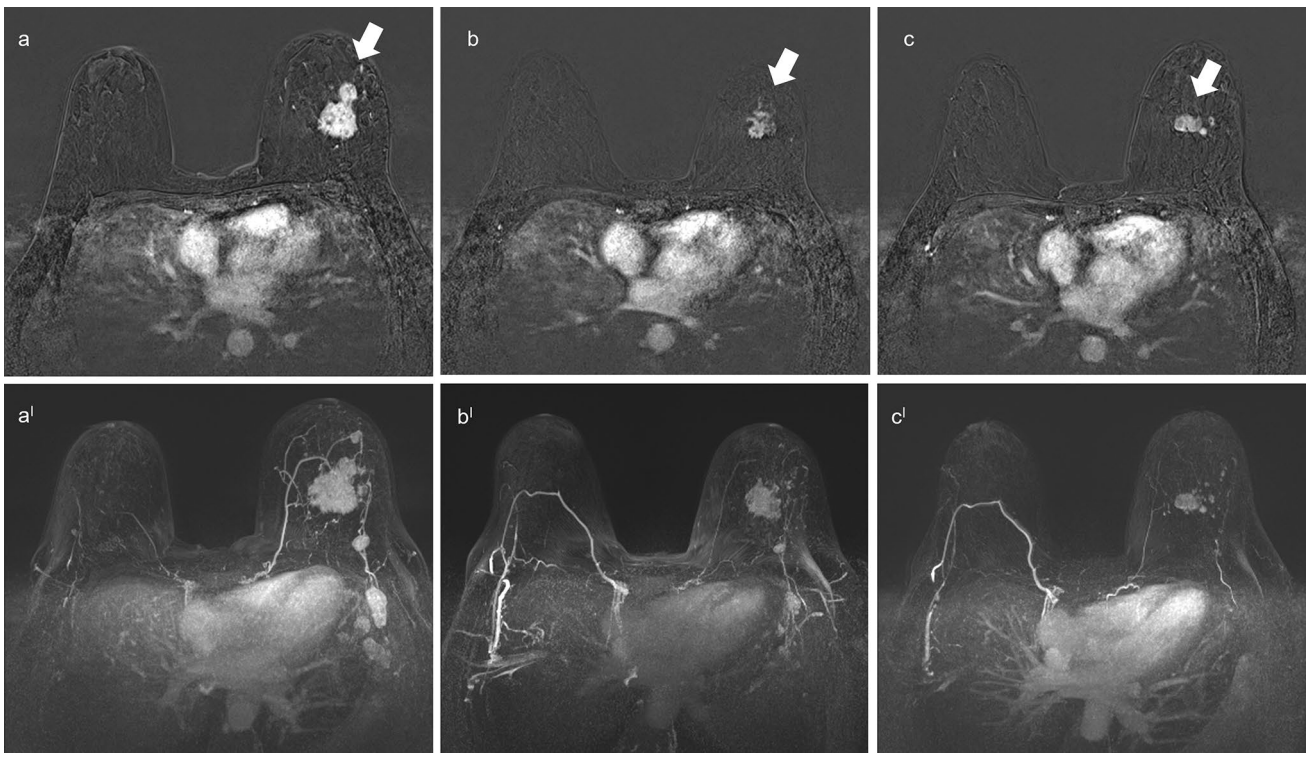

Fig. 5 Axial images from breast MRI in a 59-year-old woman with an invasive ductal carcinoma of the left breast. **a;aI** Image from pre-chemotherapy contrast-enhanced T1-weighted subtraction image MRI and MIP shows an irregular enhancing mass associated with some satellite masses in a multicentric lesion. The maximal diameter of the index mass was measured as 4.8 cm (white arrow). **b;bI** On image obtained after the completion of six cycles of chemotherapy, the mass shows a concentric shrinkage pattern (white arrow). It is suggestive of partial response **c;cI** Image from post-chemotherapy shows a further dimensional reduction, always suggestive of partial response (white arrow). Surgical histopathologic examination revealed a 2.0-cm invasive ductal carcinoma

Breast

Tissue characterization

DCE-MRI is the most accurate imaging modality in the evaluation of mass and non-mass breast lesions, to obtain morphological and kinetic information with high spatial and temporal resolution [16, 82, 83]. Typical breast cancer demonstrates an intense and rapid contrast enhancement and contrast wash-out, due to increased angiogenesis, capillary permeability, and shunts [16, 84]. Kuhl et al. have identified three main patterns of the TSI curves: type I – progressive (lowest probability of malignancy); type II – plateau (intermediate probability); and type III – wash-out (high

probability) [85]. When the same lesion has different kinetic patterns, it is advisable to consider the most suspicious. Notably, the evaluation of the kinetic curves must always be associated with a morphological evaluation of the lesion [86] (Fig. 4). Kinkel et al. reported that the combined evaluation of dynamic kinetic curves and morphological characteristics improved the diagnostic performance of DCE-MRI (sensitivity of 97%, specificity 96%), compared to dynamic kinetic curve evaluation alone (sensitivity of 85%, specificity 87%) [87]. In addition to the qualitative evaluation of enhancement, a quantitative pharmacokinetic evaluation can be performed. Calculation of Ktrans and Kep has been shown to improve the distinction between malignant and benign lesions, reducing the number of false positives and unnecessary biopsies [88]. Recent developments in breast MRI include abbreviated and ultrafast MRI. Abbreviated MRI refers to the shortening of a standard breast MRI protocol, maintaining a single contrast sequence of shorter duration and a limited number of other sequences [89]. Ultrafast MRI refers to a distinct new sequence of images, with high temporal resolution (typically 6–7 seconds), developed to acquire the early stages of the influx of contrast medium into breast lesions [89]. Ultrafast MRI is currently highly experimental, including kinetic parameters that are different from traditional and abbreviated breast MRI.

Tumor response assessment

DCE-MRI is the most accurate imaging modality for assessment of tumor response to neoadjuvant chemotherapy [90].

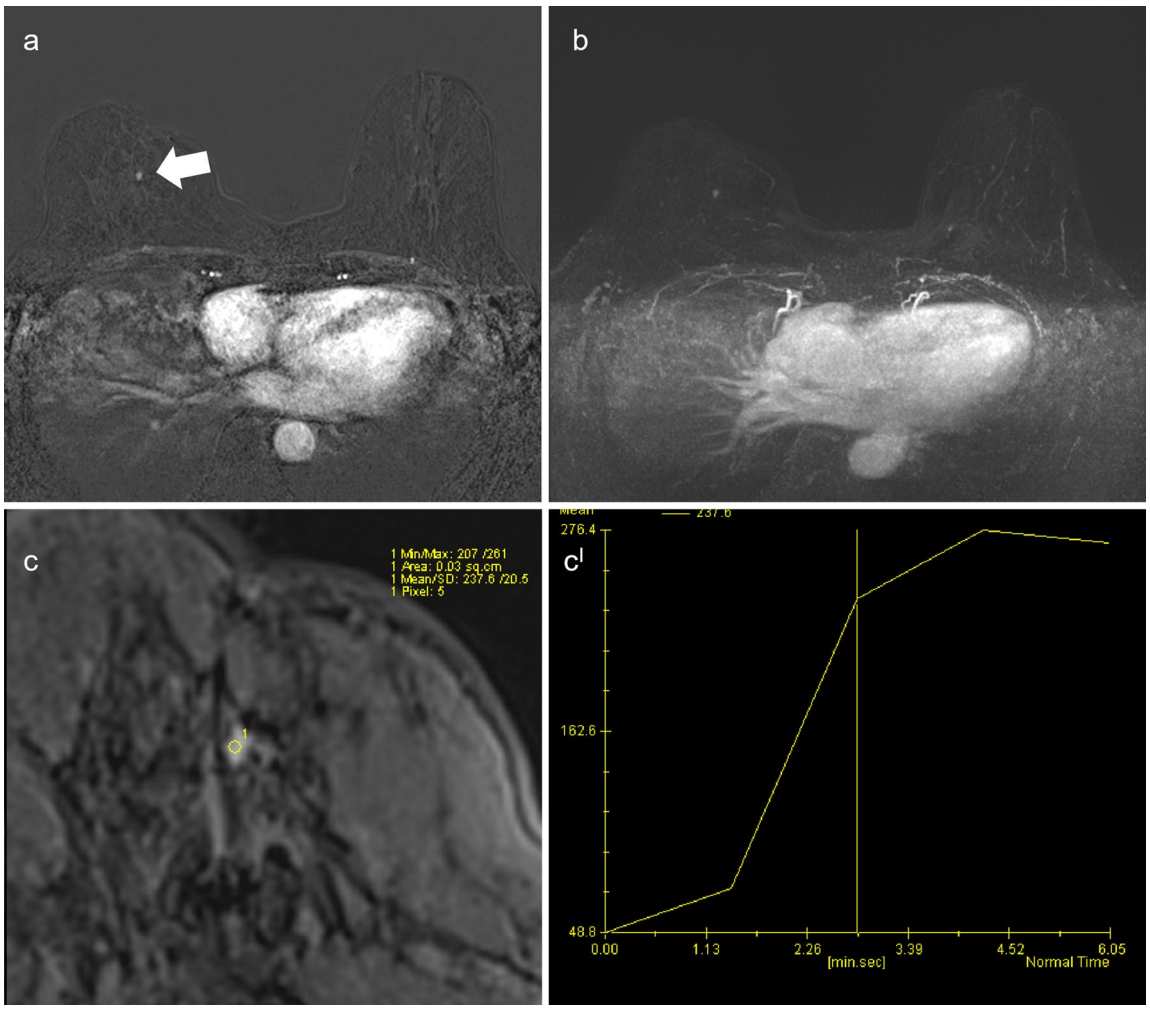

Fig. 6 A case of recurrent breast cancer after conservative surgery using post-operative MRI. A 51-year-old woman, who had right breast conserving surgery for invasive lobular carcinoma 4 years ago, recent mammography finding of suspicious opacity in the scar site without an ultrasound fee. The patient underwent ce-MRI. Dynamic contrast-enhanced subtracted image and MIP **a; b** demonstrated 6.0-mm irregular mass (white arrow) in the site of the post-operative scar. **c;cI** Time–signal intensity curve of the mass shows a rapid enhancement and mild decrease in the late phase. Tomosynthesis-guided vacuum assisted biopsy of this lesion showed recurrent invasive lobular carcinoma

Both changes in maximum tumor size, tumor volume, and enhancement kinetics at imaging and functional techniques have been investigated [91] (Fig. 5). The change in tumor volume, also measured with the aid of semiautomatic Computer Assisted Diagnosis (CAD), showed the strongest predictive performance for pathological complete response after the first cycle of neoadjuvant chemotherapy and has the strongest association with relapse-free survival [92]. Also an early decrease in enhancement in the analysis of the TSI curves is an important predictor of possible response to therapy [93, 94] (Fig. 6). DCE-MRI may be considered as a method of evaluating suspected recurrence by either clinical examination, mammography or ultrasound [95]. In case of relapse this will appear in DCE-MRI as a new malignant lesion with intense enhancement and wash-out kinetics, while a scar with fibrous tissue shows absence or slight enhancement with progressive kinetics [96]. DCE-MRI is the diagnostic technique with the greatest sensitivity in identifying local relapse, and can be used to exclude the presence of malignancy, thanks to the high negative predictive value demonstrated, avoiding unnecessary biopsies [97, 98].

Lung

Techniques

Several methods are currently available to quantitatively and qualitatively assess lung perfusion in patients with different conditions, in particular dual-energy computed tomography (DECT), dynamic contrast-enhanced perfusion CT (DCECT), time-resolved contrast-enhanced magnetic resonance angiography (CEMRA), and DCE-MRI [99–101]. DECT can provide perfusion-based information through iodine distribution map, using CT scanners with specific X-ray production, in order to obtain CT data from low-energy and high-energy X-ray spectra [100, 102]. With ADCT (area-detector CT), isotropic volume data of pulmonary parenchyma, nodules, or masses can be obtained simultaneously in an area of 160 mm without helical scanning. In routine clinical practice, dynamic contrast-enhanced perfusion ADCT are usually evaluated in the form of quantitative maps of perfusion parameters by means of mathematical models [100, 103].

The introduction of time-resolved 3D (or 4D) CEMRA has allowed increasing the spatial resolution to the same level as pulmonary CT angiography (CTA) and improving the temporal resolution to less than 5s by using parallel imaging techniques [104]. Therefore, time-resolved CEMRA is currently one of the best MRI techniques for assessing the pulmonary vascularization and perfusion in pulmonary parenchyma of patients with various pathological conditions [104, 105].With DCEMRI, multiple images can be obtained during the first passage with an intravascular contrast agent through the pulmonary circulation. Images are generally acquired using a 2D or 3D dynamic gradient-echo sequence with ultrashort echo time and repetition time, necessary to overcome signal loss due to the inhomogeneous magnetic susceptibility of lung parenchyma [106]. This method provides regional pulmonary blood flow (PBF), pulmonary blood volume (PBV), and mean transit time (MTT) within the whole lung and demonstrates the regional differences for each perfusion parameter in both normal and pathological lung conditions [106, 107].

Clinical applications

DECT technique nowadays is commonly used to rapidly obtain perfusion maps within the lungs in patients with pulmonary vascular diseases, in particular acute/chronic

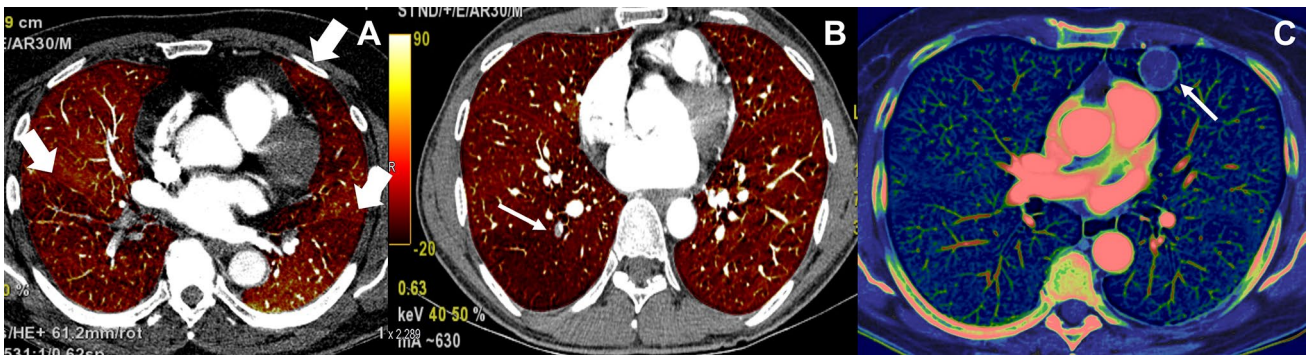

Fig. 7 Examples of perfusion studies with Dual Energy CT (DECT). Two examples of lung perfusion in chronic (**A**) and acute (**B**) pulmonary thromboembolism: color-coded lung perfused blood volume map and CT images from 80kVP and 140 kVp were fused by commercial software. Thrombi in central zones (thin arrow) and peripheral ones (large arrows) are clearly demonstrated as defects within pulmonary perfusion. Image in C shows a perfusion study of a solid nodule (arrow): this is characterized by minimal/absent vasculature and histology confirmed the hamartomatous nature

pulmonary embolism, as well as nodules/masses (Fig. 7). Several studies have reported that DCECT has a sensitivity between 93 and 100%, specificity of 52–93%, and accuracy of 77–97% in differentiating malignant from benign lung nodules. DCE-MRI has not demonstrated significant differences in diagnostic performance for lung nodules compared to DCECT, so these methods may have a complementary role in this setting [108]. CT and MRI perfusion have been shown to have equal diagnostic value in assessing response to conservative therapy in lung cancer compared to 18F-Fluorodeoxyglucose positron emission tomography (18F-FDG-PET) [109]. Indeed, perfusion imaging parameters can be used as biomarkers of response in this condition in the same way as glucose metabolism data, providing information on changes in the angiogenetic status of the lesion [110]. Time-resolved CEMRA was proposed as a new tool for the diagnosis of pulmonary thromboembolism having higher sensitivity than CTA (83% versus 75%) in its detection [111]. Although with lower spatial resolution, perfusion MRI is more sensitive than time-resolved CEMRA in the detection of subsegmental thromboembolic defects, shown by indirect visualization of lung parenchymal perfusion alterations [112]. Finally time-resolved CEMRA and MRI perfusion can be used also as quantitative assessment methods in the setting of pulmonary hypertension, in particular in near future they may have a complementary role in routine clinical practice for grading disease severity as well as evaluating its progression [107].

Heart

DCE in cardiac patients has been used for the evaluation of myocardial perfusion (MP). During the latest years, MP imaging (MPI) has achieved a pivotal role in the approach to ischemic heart disease (IHD) since ischemic-guided therapy functional assessment of coronary artery disease (CAD) proved superior to the anatomical evaluation of CAD in the treatment of stable angina patients [113]. PET was the first technique to establish the estimation of Myocardial Blood Flow (MBF). However, with the new technologies, Cardiac MRI and CT resulted highly advantageous in perfusion imaging. Cardiac MRI and CT benefit from wider accessibility, lower costs, and a comprehensive application in cardiomyopathies and IHD [114–132]. High diagnostic accuracy of both stress-rest Cardiac MRI and CT-MPI in identifying ischemia using vasodilating agents is widely demonstrated [133–138]. However, although ischemia has shown important prognostic value, the burden of ischemia has recently become an important focus [139]. In this regard, SPECT and PET were able to provide a quantitative evaluation of MBF. Conversely, from the standard of reference, qualitative data were extrapolated for MRI and CT [140]. However, although the good accuracy of qualitative and semi-quantitative analysis, most recently, quantitative assessment proved the highest accuracy in identifying ischemia. MPI indeed can distinguish multivessel disease or balanced ischemia only with a quantitative approach. Different mathematical models have been investigated for quantitative estimation of MBF, showing a non-significant difference between models, although the most technically applicable is recommended [141]. However, current improvement in analysis, including artificial intelligence quantification of perfusion mapping, provides a strong impact in predicting major adverse cardiac events (MACE) [22, 142]

Stress cardiac MRI

Current Cardiac MRI protocols allow the acquisition of three short-axis at each heartbeat for about 50–60 consecutive heartbeats. The temporal resolution of DCE-Cardiac MRI is approximately 1 second. The temporal and spatial resolution has also been increased through the introduction of 3D whole-heart acquisition [141, 143]. Clinical impact of stress Cardiac MRI resulted similar to the current gold standard in the functional evaluation of dynamic changes of coronary flow (i.e., Fractional Flow Reserve or FFR). MR-INFORM trials highlighted a non-inferior validity of stress Cardiac MRI to FFR in predicting MACE in patients with stable angina [144]. Two recent papers confirm high impact of quantification of ischemic burden in stress Cardiac MRI. In a large retrospective registry, including 6389 patients of Marcos-Garces et al., extensive ischemic burden was related to a higher risk of long-term, all-cause mortality, and efficacy of revascularization strategy also appeared related to the extensive ischemia [145]. On the other hand, in a recent paper of Sammut et al., quantitative analysis confirmed an incremental prognostic value to visual assessment and established risk factors in a patient population of 395 patients with suspected CAD [146].

CT-MPI

Dynamic and static acquisition can be performed for CT-MPI, varying widely also in temporal resolution and diagnostic accuracy. In static technique, a single acquisition samples the first pass of contrast in the myocardium. Conversely, in the dynamic shuttling mode, the acquisition is repeated for about 20–30 consecutive heartbeats. Surely, temporal resolution of CT-MPI depends on scanner technology. CT-MPI with wider detectors (able to acquire 16 cm volumes) can acquire the whole heart in a single heartbeat. Temporal resolution in 320-row scanners is one half the gantry rotation time, which turn in the order of 135 ms in second generation scanner using

a prospective acquisition; otherwise, in the dynamic shuttling mode, the temporal resolution has been increased also using the dual-source technology (up to 63 ms) [141, 147, 148]. In static CT-MPI, scan timing is crucial for detecting perfusion abnormalities. However, many factors could influence optimal scan time and prospective estimation of the optimal scan timing remains challenging [149]. Otherwise, dynamic acquisition is independent on scan time. Moreover, dynamic techniques only allow quantifying MBF. Other differences regard dose exposure and longer acquisition. However, latest scanners allow significant reduction not exceeding 5 mSv, and rigid and non-rigid transformation techniques can be applied to realign cross-section misalignment consequent to motion artifact [141]. Two considerations must be added: 1) diagnostic validity of CT-MPI is comparable to other perfusion techniques as shown in the meta-analysis by Takx et al. [150]; 2) clinical utility of CT-MPI in discriminating functional significance of CAD increases when CT-MPI is complementary to coronary CT or FFR-CT, becoming comparable to invasive quantification, both in a routine clinical setting as showed in the CORE320 recent SPECIFIC multicenter study by Nous et al., or in an emergency setting as shown by Granghi et al. in patients with acute chest pain [151, 152].

Liver

DCE liver studies with CT and MRI provide a quantitative estimation of the blood transport across a tissue at the capillary level [153, 154]. After a pre-contrast acquisition, the typical CT protocol includes a first-pass phase (for 45–60 s with a temporal sampling <1.5s) and a delayed phase (for up to 2 minutes with lower temporal resolution and depending on the model) [155]. The injected amount iodinated contrast agent (≥300 mgI/mL) should be of 30–60 mL at a rate >4 mL/s, followed by a saline chaser [156]. To obtain an adequate dataset, several strategies are used in CT. If the detector has a wide coverage along the z-axis and the X-ray tube has an optimal performance, sequential acquisitions with low kV, high mA, and high temporal resolution are used; however, sequential spiral acquisitions can be implemented to achieve a wider anatomical coverage (>20 cm) [155]. In MRI, the DCE studies of the liver face several technical challenges (anatomical coverage and respiratory motion), solved by the recent technical advances. Usually, a 3D, T1w, fast spoiled GRE is preferred, with parallel imaging for adequate temporal resolution better temporal resolution (≈1.9s per slab) [19, 23]. The T1 mapping is necessary for the quantification of gadolinium concentration, and oblique slices, including the aorta and portal vein, are preferred for subsequent analysis [19]. A relatively new technique is the golden-angle radial sparse parallel (GRASP) DCE MRI: the technique involves a non-cartesian radial sampling of k-space with a golden-angle scheme to obtain high signal of the liver parenchyma at free-breathing. The use of parallel imaging allows for adequate temporal resolution for DCE-MRI of the liver (1.5s) [157, 158]. Different models have been developed for perfusion analysis. The model-free maximum-slope analysis uses the peak enhancement of the spleen to separate the arterial and portal perfusion of the liver and to calculate semi-quantitative parameters (e.g., Arterial Liver Perfusion or Hepatic Perfusion Index) [159] (Fig. 8). When studying tumor vascularity, the compartmental modeling is helpful, in particular for the investigation of neoangiogenesis during hepatocarcinogenesis or perfusion of liver metastases [160, 161]. The dual-compartment models consider the vascular and the extravascular spaces as separate; the distributed models consider the diffusion gradients of the tracer across the compartments [162, 163]. Several reports have demonstrated the role of DCE in early detection and characterization of liver lesions [164, 165], both for hepatocellular carcinoma on cirrhosis (166-170) or for the early detection

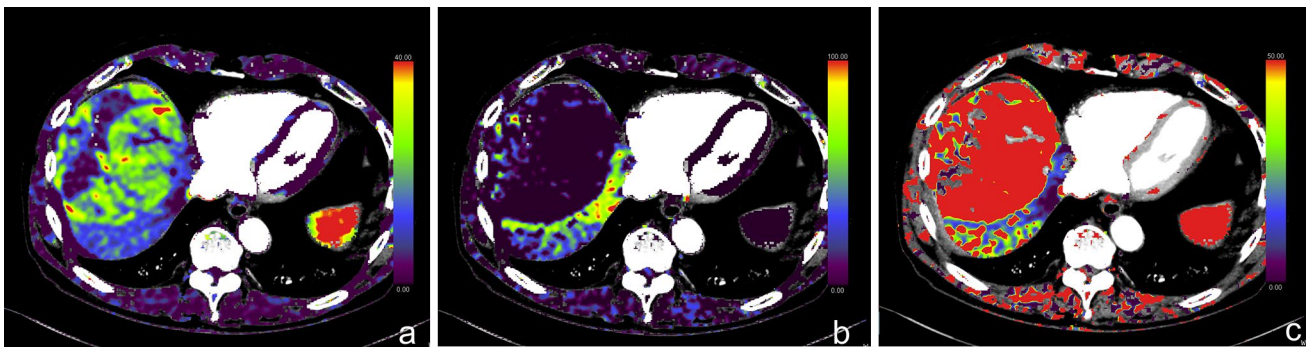

Fig. 8 Volume Perfusion CT, male, 67 years old, hepatocellular carcinoma. A-c: model-free maximum slope. The hepatocellular carcinoma has significantly higher arterial perfusion (**a**) and lower portal perfusion (**b**) than the surrounding parenchyma, resulting in a higher hepatic perfusion index (**c**)

of metastases where perfusion changes may precede the occurrence of the lesion [5, 171]. The assessment of perfusion parameters also demonstrated clinical utility in the prediction or early assessment of treatment response of tumor primary or metastatic liver tumors, where the perfusion changes may be the only sign of treatment response, or for prognostication of disease progression [172–177]. Moreover, perfusion changes in sites of locoregional treatments may be predictive of tumor recurrence, in particular for metastases [178]. Finally, perfusion changes have been correlated to the degree of fibrosis in chronic liver diseases [179, 180].

Pancreas

The main application of CT and DCE-MRI in pancreatic pathology is for assessing pancreatic cancer [24, 162, 181–188]. Hu et al conducted a study to evaluate inflammatory processes [189]. The ability to evaluate the angiogenesis activity allows critical future developments in the oncology field [190–192]. Compared to conventional CT, DCE-CT requires higher radiation exposure and more time to process data [193]. Depending on the kinetic model and the desired perfusion parameters, different scans are performed before, during, and after the injection of iodinated contrast medium [162]. DCE-MRI involves the administration of a contrast agent (gadolinium chelate) and the assessment over a selected region of interest (ROI) of signal intensities changes over time (TICs) [1, 194]. Motosugi et al. hypothesized that gadoxetic acid-enhanced MRI would be useful for assessing pancreatic carcinoma because it would be able to depict pancreatic lesions through intrinsic T1 contrast and small liver metastases through the contrast of the liver-specific agent [195]. Several studies have shown significant differences between patients with pancreatic cancer, neuroendocrine pancreatic cancer, and chronic pancreatitis [196, 197]. Bali and colleagues evaluated patients with surgery resectable pancreatic lesions and demonstrated different values between malignant tumors versus benign lesions and non-cancerous pancreatic tissue [198]. Coenegrachts et al. explored the potential of DCE-MRI for chronic pancreatitis [199]. In addition, a study was conducted where the measurement of pancreatic signal intensity in DCE-MRI proved helpful in diagnosing early or mild chronic pancreatitis, especially before any apparent changes in morphological or pancreatic signal intensity [200]. Pancreatic perfusion can undoubtedly be influenced by age, by the presence of degeneration, such as fatty infiltration, periductal and lobular fibrosis, and hyperplasia of the ductular epithelium [199]. Importantly, Akisik et al, found that DCE-MRI can predict which pancreatic tumors will have a good response to antiangiogenic therapy [201]. For the future, it is necessary to create pharmacokinetic models on which to base the semi-quantitative analysis of lesions.

Gastrointestinal

DCE-MRI is a currently evolving imaging application for the gastrointestinal system and not only for oncological imaging [186, 202].

Gastric cancer

Several studies (203-206) have focused on assessing the aggressiveness, staging, Lauren's type classification of gastric cancer (GC), and prognosis and response to therapy. Joo et al. (203), as well as in another similar study Ma et al. [204], evaluated the correlation of quantitative parameters, in particular of Ktrans, with the expression levels of epidermal growth factor (EGFR) and vascular endothelial growth factor (VEGF), which are two of the main angiogenic factors. A high Ktrans value is correlated with increased expression of molecular markers and thus a higher degree of angiogenesis. These results suggest that DCE-MRI reflects tumor biology and perfusion dynamics and provides important prognostic information [207]. Furthermore, in a recent study [208], quantitative DCE-MRI parameters (Ktrans and Kep) were shown to be independent predictors of extramural venous invasion in patients with locally advanced gastric cancer.

Rectal cancer

DCE-MRI is also a promising method for rectal cancer (RC). Studies have focused on the ability of quantitative and semi-quantitative parameters to detect residual tumors after neoadjuvant chemoradiotherapy in patients with locally advanced cancer [209–212]. Others focused on the reliability of DCE-MRI in predicting complete pathological response before neoadjuvant chemoradiotherapy in patients with locally advanced cancer, although with Ktrans cut-off values varying between studies (0.32 min-1 and 0.66 min-1) [209, 213–216]. Other studies [217–222] have correlated DCE parameters with tumor staging and aggressiveness, but there were conflicting results. Similar studies on response to treatment but involving ultrasound have also been carried out for GISTs. For example, one study [223] showed that reduced values at DCE-US (at day 7) were highly predictive of ^{18}F-FDG-PET results (at one month).

Inflammatory bowel disease

Finally, the DCE-MRI role is now also recognized for chronic inflammatory bowel diseases [181, 183, 224, 225]. Vieujean et al. [226] investigated the role of DCE-MRI in affected and unaffected segments in patients with Crohn's disease (CD) and compared them to a control group, suggesting complex perfusion changes in both intestinal parts (affected and unaffected) in CD. Others, however, have shown a correlation with CD activity status [20, 227–229], with clinical scores and laboratory data [226, 228–230] and the response to treatment [231, 232]. One study has shown that perfusion analysis using DCE-US 1 month after treatment in patients with CD can provide prognostic information on treatment efficacy [233]. Although the acquisition of functional data regarding the gastrointestinal system is marred by numerous movement artifacts related to respiration and intestinal peristalsis, some studies [203, 234] have attempted to increase the spatial and temporal resolution of MRI to overcome these limitations. However, to date, it is widely accepted that quantitative surrogate parameters of tumor biology assessed by imaging still require extensive standardization and validation in clinical practice.

Gynecology

DCE in gynecological malignancies is mainly applied to endometrial, cervical, and ovarian carcinomas [235].

Ovarian masses

DCE is useful for characterizing ovarian masses [236]. In this regard, Li et al. analyzed TIC and DCE semi-quantitative parameters of 102 complex ovarian lesions (71 malignant, 16 borderline, and 15 benign). The analysis revealed that type III TIC was significantly specific for malignant tumors. Maximum slope was significantly higher in malignant than in borderline and benign tumors and time of half rising (THR) was significantly different, in ascending order, in malignant, borderline and benign tumors [237]. Turkoglu S et al. analyzed 43 ovarian masses (20 benign and 23 malignant) and found that volume transfer constant (Ktrans) was lower in benign tumors than in malignant ones and rate constant (Kep) and iAUC were greater in malignant than in benign [21].

Endometrial and cervical cancer

For staging endometrial cancer T2W images are usually sufficient in showing disruption of myometrium; however, in postmenopausal patients reduction of zonal differentiation may make more difficult to assess myometrial infiltration [7]. DCE in sagittal plane, in such cases, improves the detection of small tumors, given the earlier enhancement if compared to the normal endometrium, and the accuracy of the depth of myometrial invasion by increasing contrast resolution between cancer and myometrium on equilibrium phase [238–240] (Fig. 9). Moreover, DCE may solve the dilemma between cervical stromal invasion and tumor protrusion into the endocervix on T2W sequences [241] and is helpful for differentiating cancer grade. In fact, quantitative parameters (relative enhancement, maximum enhancement, and maximum relative enhancement) are significantly higher in G1 than in G2 and G3 tumors [242]. Concerning the staging of cervical carcinoma, DCE is deemed unnecessary, although it may improve confidence of inexperienced reader in detection of stromal and parametrial invasion [238].

DCE is effective for evaluating response to chemoradiotherapy in FIGO stage II–IV cervical cancers. In fact it has been demonstrated that high perfusion values before and during radiation therapy are indicative of high tumor oxygenation and therefore of better prognosis [243, 244]. Zhang

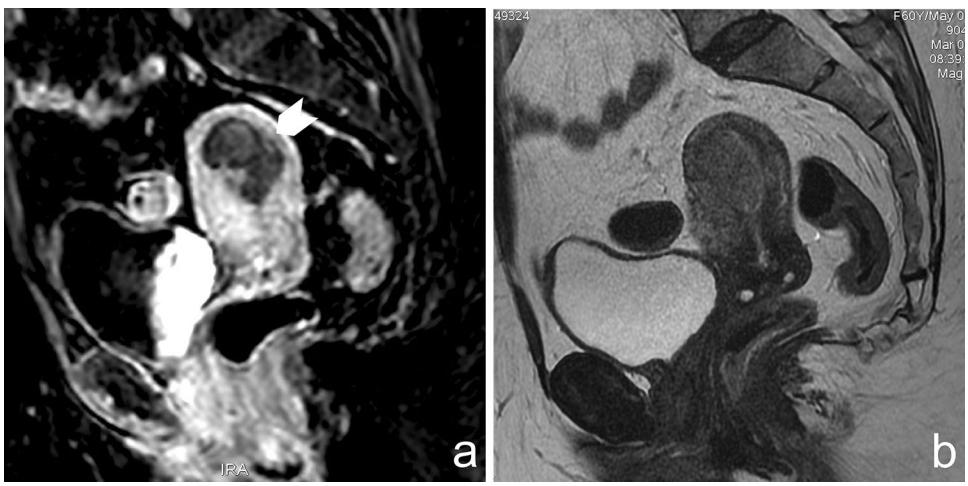

Fig. 9 A 61-year-old woman with an endometrial carcinoma infiltrating more than 50% of myometrium. Post-contrast sagittal T1W images (arrow in **a**), if compared to T2W (**b**), improves the contrast resolution between the cancer and myometrium

Z et al. performed pelvic DCE-MRI of 108 patients with advanced cervical carcinoma before treatment and found that Ktrans was higher in responders than in non-responders both in the center and in the periphery of tumor, whereas Kep was significantly higher in responders only in the periphery of lesion. The higher capability of perfusion parameters in the peripheral region to predict treatment response is explained by the fact that the center of tumor if frequently necrotic may not be representative of the overall tumor vascularization [245, 246]. On the contrary, persistent contrast uptake at completion of therapy may be indicative of residual disease; however in such case, DCE should be integrated with DWI for differential diagnosis with post-actinic inflammation [247–249]. DCE is useful for identifying local recurrence in cervical and endometrial cancers because conventional MRI is limited by treatment effects on normal pelvic anatomy. Pathological tissue shows usually an early enhancement peak followed by wash-out, allowing a confident diagnosis [249].

Kidney and bladder

Renal perfusion assessment

DCE-US, CT, and MRI of the kidney provide multiple functional parameters, such as renal perfusion and glomerular filtration rate [9]. DCE-US can assess the microcirculation using phospholipid-based microbubbles as intravenously injected contrast agent [2]. These bubbles, unlike the ionic agents used for CT and MR, are purely intravascular and are eliminated via the respiratory system [250]. DCE-US allows only semi-quantitative measurements of renal perfusion, analyzing the TIC (250, 251). The TIC obtained with non-diffusible agents has only a vascular peak followed by recirculation (Fig. 10) [9]. The great advantages of this technique are the low costs, the use of non-nephrotoxic contrast agents, and the absence of ionizing radiation.

DCE-US for monitoring tumor response to antiangiogenic treatment has been standardized by several authorities [2, 252]. DCE-CT and DCE-MRI allow both semi-quantitative and quantitative analyses and provide measurement of both

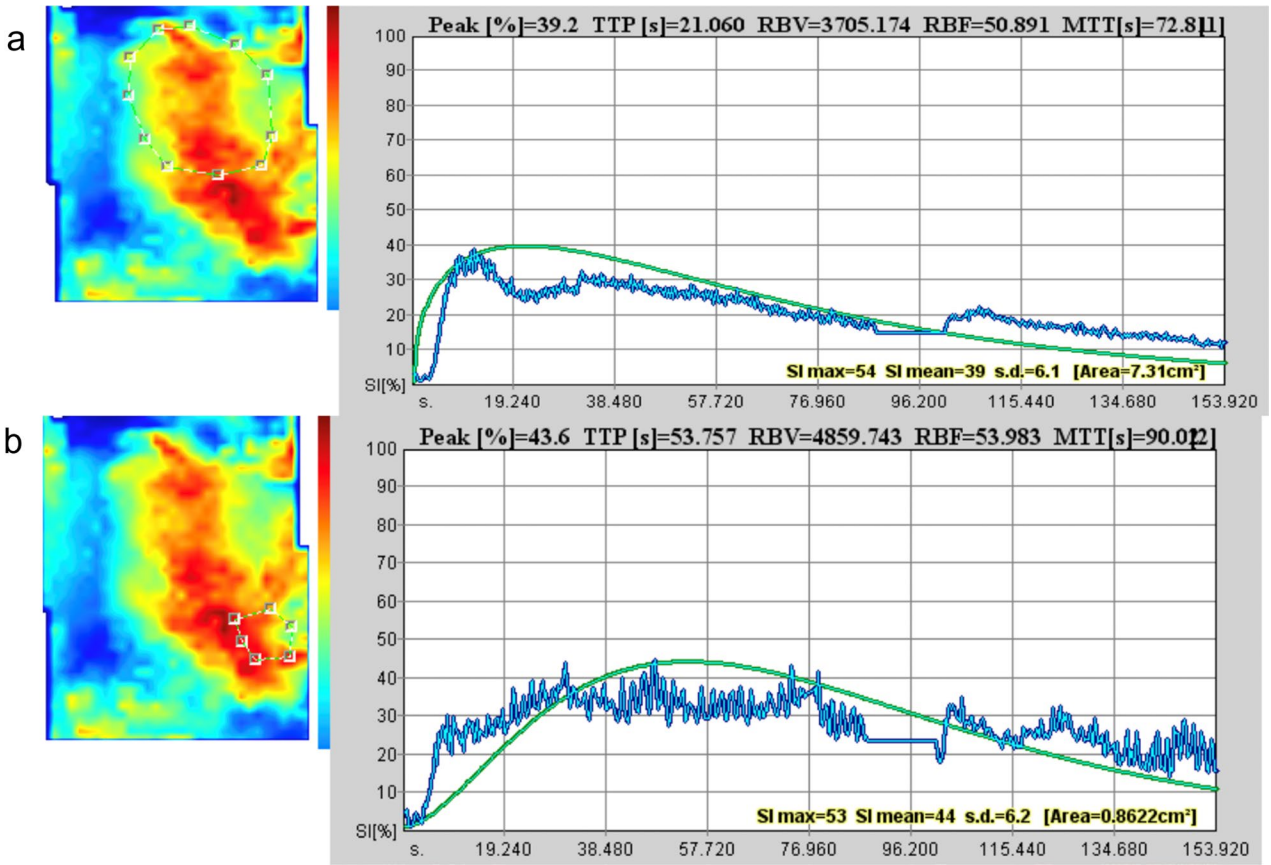

Fig. 10 **A** Typical signal–time curve obtained in a normal kidney after injection of non-diffusible microbubbles with a rapid wash-in phase followed by a slow wash-out phase. **B** Signal–time curve obtained in a malignant renal mass with slow wash-in and very slow wash-out

renal perfusion and filtration [9]. The normal TIC obtained with the diffusible contrast agents of CT and MRI has three phases: a vascular phase with an early peak, a glomerular-tubular phase with a slow increase, and the final excretory phase characterized by a slow decay of signal intensity [253]. DCE-CT is poorly used because has several limitations: the nephrotoxicity of iodine agents, the risk of contrast agent-induced hyperthyroidism, and the radiation exposure [9, 254]. In addition, compared to DCE-MRI, temporal resolution is lower, so that quantitative data can be assessed less precisely [255]. DCE-MRI is based on dynamic acquisition during the transit of a low-molecular-weight gadolinium contrast agent through the renal cortex, medulla, and the collecting system [9, 253, 256]. The most used sequence is a fast 3D-spoiled GRE T1-weighted sequence, acquired in an oblique coronal plane through the long axis of the kidneys [253]. A temporal resolution of at least 4s and a total acquisition time of at least 4 min are necessary to measure both perfusion and filtration processes [255]. DCE-MRI of the kidney has many clinical applications [9]. DCE-MRI can be required to measure single-kidney glomerular filtration rate if renal asymmetry is associated with a reduced renal function, before renal surgery or biopsy [257]. Michaely et al. found that DCE-MRI allows to distinguish between high- and low-grade renal artery stenosis [258]. Most studies have evaluated functional side of imaging in non-vascular renal disease identifying abnormal perfusion values if microvascular or macrovascular blood flow is impaired [253, 259]. DCE-MRI is useful in differential diagnosis between acute tubular necrosis and acute renal allograft rejection, where cortical and medullary perfusion parameters are reduced [260]. Functional imaging could help in the histological differentiation of renal masses [261–264]. Response to antiangiogenic therapy can be evaluated early by DCE-MRI. Several studies have demonstrated that in patients with metastatic renal cell cancer (mRCC) tumor blood flow and permeability decrease after targeted therapy [265]. Finally, high baseline permeability correlates with prolonged complication-free survival after targeted therapy in mRCC [254].

An increased application of DCE imaging has also been observed regarding evaluation of bladder cancer (BC). Several studies analyzed the accuracy of DCE-US in distinguishing T-staging and grading of BC. Drudi et al. identified three TIC shapes that may differentiate low- and high-grade BC with a sensitivity and specificity of 91.6% and 85.7%, respectively [261]. DCE-MRI of the bladder is based on dynamic acquisition of fat-suppressed 3D-T1W-spoiled GRE images after gadolinium injection with variable imaging planes [266, 267]. A temporal resolution of at least 10 s and a total acquisition time of at least 5 min are recommended.

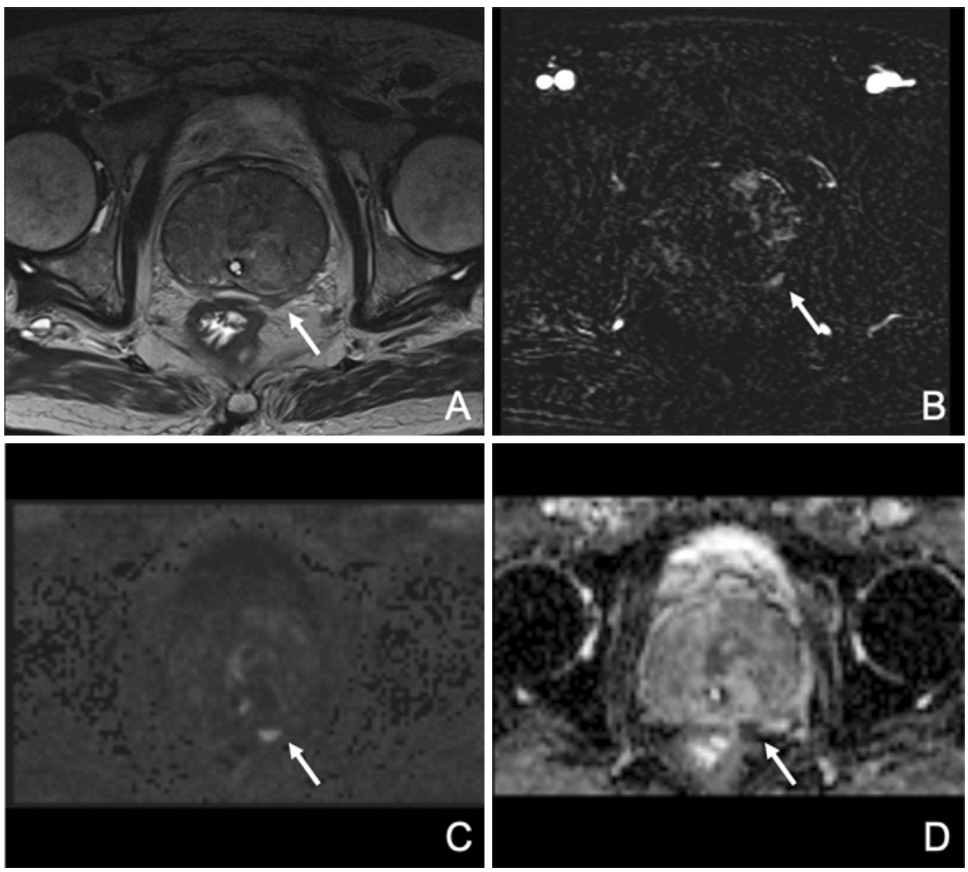

Fig. 11 Focal alteration of the intermediate left PZ scored as a PI-RADS 4: **A** axial view of T2W showing a low signal alteration in the PZ (white arrow); **B** axial view of DCE on 3D T1W GRE image evidencing an early enhancement in correspondence of the alteration in the PZ (white arrow); **C** axial view of DWI (b 1500) showing a hyperintense alteration in the PZ (white arrow); **D** axial view of ADC map showing a hypointense alteration in the PZ (white arrow)

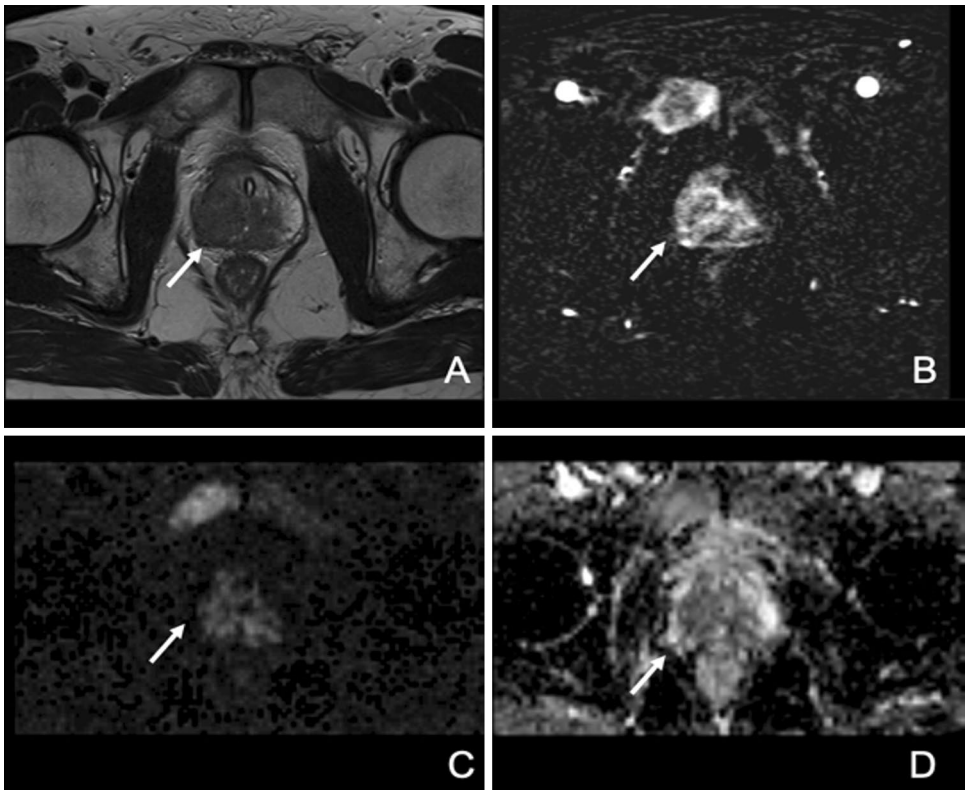

Fig. 12 Alteration of the intermediate right PZ and TZ scored as a PI-RADS 5: **A** axial view of T2W showing a low signal alteration in the PZ and TZ (white arrow); **B** axial view of DCE on 3D T1W GRE image evidencing an early enhancement in correspondence of the alteration in the PZ and TZ (white arrow); **C** axial view of DWI (b 1500) showing a hyperintense alteration in the PZ and TZ (white arrow); **D** axial view of ADC map showing a hypointense alteration in the PZ and TZ (white arrow)

BCs show an early enhancement, along with the bladder mucosa, and lamina propria, whereas the underlying detrusor muscle demonstrates a delayed enhancement [266]. In literature, the accuracy of DCE-MRI in BC staging varied widely ranging from 52 to 93% [18, 268]. Zhou et al. demonstrated that apparent diffusion coefficient value and DCE-derived tumor wash-out may be associated with higher-grade cancer [269].

Prostate

Prostate DCE and PI-RADS

In latest years multiparametric MRI (mpMRI) has been more and more applied in the diagnosis, therapy, and treatment response of Prostate Cancer (PCa) [270–274]. The images are evaluated in accordance with the Prostate Imaging Reporting and Data System version 2.1 (PI-RADSv2.1) [275]. In PI-RADSv2.1 the use of DCE-MRI is recommended and the findings should be considered positive when there is a focal enhancement, earlier or contemporaneous with the enhancement of adjacent normal prostatic tissues, with a corresponding alteration on T2-weighted (T2W) and/or DWI sequences [275–277] (Figs. 11 and 12). PI-RADS v2.1 specifies that DCE-MRI can be performed with both two-dimensional and three-dimensional T1-weighted (T1W) GRE acquisitions; however, it suggests a preferred use of the three-dimensional T1W GRE, for a better signal-to-noise ratio. It recommends also to use a temporal resolution of 15 s, in order to maintain a good quality of the image [278]. The most available method to evaluate DCE is the direct visual assessment of enhancement. Curve analysis or production of colorimetric maps is not supported in clinical use due to the lack of scientific evidence [275]. Although DCE-MRI has demonstrated to have high sensitivity and specificity in detecting PCa, its use in assessing the score of prostatic alterations is still limited [278, 279]. DCE-MRI becomes crucial, if positive, to categorize, as a PI-RADS 4, a suspicious finding in the peripheral zone with T2W and DWI scores of 3. On the other hand, it still does not have any use in scoring alterations of the transitional zone [275, 278, 280]. Literature has shown that DCE-MRI contributes in the detection of PCa in both peripheral zone and transitional zone, and is an important tool when other sequences are inadequate for artifacts. In the evaluation of DCE-MRI findings the radiologist must be aware of possible PCa mimics and should recognize them, such as central zone and anterior fibrovascular stroma, thickening of the surgical capsule, periprostatic venous plexus, post-biopsy hemorrhage, stromal benign prostatic hyperplasia nodules, prostatitis, post-inflammatory scars, calcifications, and atrophy [276, 280–283].

Imaging monitoring and follow-up

DCE-MRI has a crucial role in detecting recurrent or residual diseases [8]. The localization of the residual or recurrent PCa varies depending on the treatment; the most common sites are the vesicourethral anastomosis and surgical margins. The disease is presented as a solid nodule, with an early enhancement, that corresponds to a low signal alteration on T2W [8, 281]. DCE-MRI is fundamental to differentiate recurrent PCa from physiological post-operative fibrosis, which appears as a low signal alteration on T2W but in DCE-MRI shows low or absent enhancement. After radiotherapy, the prostate reduces its dimensions and presents a diffuse decreased signal on T2W, due to the presence of fibrosis. The localization of residual disease is challenging on T2W, so DWI and DCE-MRI are necessary to detect it. Residual or recurrent PCa is normally located in the site of prior tumor, presenting itself as an early enhancing nodule on DCE-MRI [281, 284]. Latest studies have evidenced a potential role of DCE-MRI in the evaluation of blood flow distribution and kinetics of the enhancement, analyzing also possible associations with Gleason Score of the lesion [285, 286]. These data might become crucial in the pre-treatment evaluation with the eventual support of Artificial Intelligence [287]. However, no significant difference has been shown yet between different Gleason Scores; meanwhile, many studies outlined that cancer lesions present higher blood flow than healthy tissue [285, 288].

Bone and soft tissues

The clinical use of DCE-MRI in the muscoloskeletal system is focused on neoplastic, infective, and rheumatic disorders [289–294].

Technique

The protocol consists of the administration of a bolus of gadolinium (0.1 mmol/kg) injected intravenously at a rate of 2 to 5 mL/second followed by a series of 15-s scans in succession, with a scan delay depending on the anatomical site (usually not exceeding 20 s) [295]. The last scan is carried out at 2 to 7 minutes depending on the protocol. DCE-MRI can provide qualitative and quantitative evaluation. A qualitative analysis consists of comparing lesion enhancement with arterial enhancement and with the neighboring tissues enhancement. However, this evaluation is too subjective to establish diagnostic criteria. Nevertheless, a qualitative approach can be useful in the evaluation of tumor margins and can better differentiate between solid and fluid-containing lesions [294].

Clinical applications

Solid neoplasms show diffuse enhancement while fluid-containing masses present smooth and non-significant enhancement at the margins. The semi-quantitative approach provides three regions of interest of identical dimensions at the site of the enhanced marked tumor, the healthy muscle, and the artery. The post-processing elaboration of TICs indicates the time from bolus arrival to the tumor site, the maximum enhancement, and the enhancement slope, allowing the classification of lesion in five different types [296]:

- Type 1: absence of enhancement (lipoma or hematoma).
- Type 2: weak and progressive enhancement (benign tumors).
- Type 3: early enhancement followed by a plateau (non-specific for a benign lesion, desmoid tumors, abscesses, and malignancy show also that type of enhancement).
- Type 4: rapid enhancement followed by a rapid washout phase (tumors with conspicuous vascular stroma and small interstitial compartment as malignant histiocytofibroma or synovial cell sarcoma, benign tumors as giant cell tumor, and osteoid osteoma).
- Type 5: rapid and vivid enhancement followed by slow and gradual enhancement (tumors with myxoid matrix and tumors after radiotherapy or chemotherapy).

Dynamic enhancement is also useful in monitoring therapeutic response. A qualitative evaluation of MRI images allows the recognition of perfused viable areas in tumor tissue within the treated anatomical site. If more than 10% of viable tumor tissue is present, a poor response to treatment is suspected [297]. From a quantitative point-of-view, at least 60% decrease in the TIC slope value indicates good response to treatment [298]. However, it is preferable to combine this with DWI, which provides complementary information in tumor evaluation [299, 300]. Another application of DCE is in suspected infectious pathologies, such as spondylodiscitis with inhomogeneous enhancement patterns at the level of disk and endplates. In cases of bone or soft tissues abscesses, DCE shows fluid collection surrounded by an irregular rim of enhancement [301]. In rheumatic diseases, such as rheumatoid arthritis, DCE-MRI is able to detect joint and tendon inflammatory processes histologically reflecting synovitis. Moreover, DCE-MRI is also able to give significant information regarding differential diagnosis between rheumatoid arthritis and psoriatic arthritis. In this setting, Schwenyer et al reported

in their study population (31 patients with rheumatoid arthritis and 14 patients with psoriatic arthritis) a statistically significant difference between the degree of synovial enhancement at fifteen minutes after contrast injection in rheumatoid arthritis and psoriatic arthritis [17]. For these reasons, the use of dynamic MRI in patients in the clinical setting of rheumatic diseases is strongly supported [6].

Conclusions

DCE imaging is widely used in whole-body imaging. In several body districts it is part of the standard MRI protocols, in others the added value has been shown for the differential diagnosis of different pathologies and a detailed characterization. The qualitative and quantitative data obtained from the dynamic contrast analysis provide essential biological tissue information, representing an important biomarker for the diagnosis and prognosis of several disorders.

Author contributions DA and FB had the idea for the article. All the authors critically revised the manuscript, commented on drafts of the manuscript, and approved the final manuscript.

Declarations

Conflict of interest The authors declare that they have no conflict of interest.

Ethical statement This article does not contain any studies with human participants or animals performed by any of the authors.

References

1. Fusco R, Petrillo A, Sansone M. Use of tracer kinetic models for selection of semi-quantitative features for DCE-MRI data classification. Appl Magn Reson. 2013;44:1311–24.
2. Lassau N, Chami L, Benatsou B, Peronneau P, Roche A. Dynamic contrast-enhanced ultrasonography (DCE-US) with quantification of tumor perfusion: a new diagnostic tool to evaluate the early effects of antiangiogenic treatment. Eur Radiol. 2007;17(Suppl 6):F89-98.
3. Lee FK, King AD, Ma BB, Yeung DK. Dynamic contrast enhancement magnetic resonance imaging (DCE-MRI) for differential diagnosis in head and neck cancers. Eur J Radiol. 2012;81(4):784–8.
4. Petralia G, Summers PE, Agostini A, Ambrosini R, Cianci R, Cristel G, et al. Dynamic contrast-enhanced MRI in oncology: how we do it. Radiol Med. 2020;125(12):1288–300.
5. Totman JJ, O'Gorman RL, Kane PA, Karani JB. Comparison of the hepatic perfusion index measured with gadolinium-enhanced volumetric MRI in controls and in patients with colorectal cancer. Br J Radiol. 2005;78(926):105–9.
6. Vordenbaumen S, Schleich C, Logters T, Sewerin P, Bleck E, Pauly T, et al. Dynamic contrast-enhanced magnetic resonance imaging of metacarpophalangeal joints reflects histological signs of synovitis in rheumatoid arthritis. Arthritis Res Ther. 2014;16(5):452.
7. Wakefield JC, Downey K, Kyriazi S, deSouza NM. New MR techniques in gynecologic cancer. AJR Am J Roentgenol. 2013;200(2):249–60.
8. Yu T, Meng N, Chi D, Zhao Y, Wang Z, Luo Y. Diagnostic value of dynamic contrast-enhanced magnetic resonance imaging in detecting residual or recurrent prostate cancer after radical prostatectomy: a pooled analysis of 12 individual studies. Cell Biochem Biophys. 2015;72(3):687–94.
9. Zhang JL, Lee VS. Renal perfusion imaging by MRI. J Magn Reson Imaging. 2020;52(2):369–79.
10. Widmann G, Henninger B, Kremser C, Jaschke W. MRI sequences in head & neck radiology - state of the art. Rofo. 2017;189(5):413–22.
11. Leithner D, Moy L, Morris EA, Marino MA, Helbich TH, Pinker K. Abbreviated MRI of the breast: does it provide value? J Magn Reson Imaging. 2019;49(7):e85–100.
12. Fabijanska A. A novel approach for quantification of time-intensity curves in a DCE-MRI image series with an application to prostate cancer. Comput Biol Med. 2016;73:119–30.
13. Petrillo A, Fusco R, Petrillo M, Granata V, Bianco F, Di Marzo M, et al. DCE-MRI time-intensity curve visual inspection to assess pathological response after neoadjuvant therapy in locally advanced rectal cancer. Jpn J Radiol. 2018;36(10):611–21.
14. Ng CS, Wei W, Bankson JA, Ravoori MK, Han L, Brammer DW, et al. Dependence of DCE-MRI biomarker values on analysis algorithm. PLoS One. 2015;10(7):e0130168.
15. Kang SR, Kim HW, Kim HS. Evaluating the relationship between dynamic contrast-enhanced MRI (DCE-MRI) parameters and pathological characteristics in breast cancer. J Magn Reson Imaging. 2020;52(5):1360–73.
16. Schnall MD, Blume J, Bluemke DA, DeAngelis GA, DeBruhl N, Harms S, et al. Diagnostic architectural and dynamic features at breast MR imaging: multicenter study. Radiology. 2006;238(1):42–53.
17. Schwenzer NF, Kotter I, Henes JC, Schraml C, Fritz J, Claussen CD, et al. The role of dynamic contrast-enhanced MRI in the differential diagnosis of psoriatic and rheumatoid arthritis. AJR Am J Roentgenol. 2010;194(3):715–20.
18. Tekes A, Kamel I, Imam K, Szarf G, Schoenberg M, Nasir K, et al. Dynamic MRI of bladder cancer: evaluation of staging accuracy. AJR Am J Roentgenol. 2005;184(1):121–7.
19. Thng CH, Koh TS, Collins DJ, Koh DM. Perfusion magnetic resonance imaging of the liver. World J Gastroenterol. 2010;16(13):1598–609.
20. Tielbeek JA, Ziech ML, Li Z, Lavini C, Bipat S, Bemelman WA, et al. Evaluation of conventional, dynamic contrast enhanced and diffusion weighted MRI for quantitative Crohn's disease assessment with histopathology of surgical specimens. Eur Radiol. 2014;24(3):619–29.
21. Turkoglu S, Kayan M. Differentiation between benign and malignant ovarian masses using multiparametric MRI. Diagn Interv Imaging. 2020;101(3):147–55.
22. Knott KD, Seraphim A, Augusto JB, Xue H, Chacko L, Aung N, et al. The prognostic significance of quantitative myocardial perfusion: an artificial intelligence-based approach using perfusion mapping. Circulation. 2020;141(16):1282–91.
23. Donato H, Franca M, Candelaria I, Caseiro-Alves F. Liver MRI: From basic protocol to advanced techniques. Eur J Radiol. 2017;93:30–9.

24. Nardone V, Reginelli A, Guida C, Belfiore MP, Biondi M, Mormile M, et al. Delta-radiomics increases multicentre reproducibility: a phantom study. Med Oncol. 2020;37(5):38.
25. Filograna L, Lenkowicz J, Cellini F, Dinapoli N, Manfrida S, Magarelli N, et al. Identification of the most significant magnetic resonance imaging (MRI) radiomic features in oncological patients with vertebral bone marrow metastatic disease: a feasibility study. Radiol Med. 2019;124(1):50–7.
26. Grassi R, Miele V, Giovagnoni A. Artificial intelligence: a challenge for third millennium radiologist. Radiol Med. 2019;124(4):241–2.
27. Neri E, Coppola F, Miele V, Bibbolino C, Grassi R. Artificial intelligence: Who is responsible for the diagnosis? Radiol Med. 2020;125(6):517–21.
28. Sourbron S, Ingrisch M, Siefert A, Reiser M, Herrmann K. Quantification of cerebral blood flow, cerebral blood volume, and blood-brain-barrier leakage with DCE-MRI. Magn Reson Med. 2009;62(1):205–17.
29. Zhang J, Liu H, Tong H, Wang S, Yang Y, Liu G, et al. Clinical applications of contrast-enhanced perfusion MRI techniques in gliomas: recent advances and current challenges. Contrast Media Mol Imaging. 2017;2017:7064120.
30. Okuchi S, Rojas-Garcia A, Ulyte A, Lopez I, Usinskiene J, Lewis M, et al. Diagnostic accuracy of dynamic contrast-enhanced perfusion MRI in stratifying gliomas: a systematic review and meta-analysis. Cancer Med. 2019;8(12):5564–73.
31. Heye AK, Culling RD, Valdes Hernandez Mdel C, Thrippleton MJ, Wardlaw JM. Assessment of blood-brain barrier disruption using dynamic contrast-enhanced MRI. A systematic review. Neuroimage Clin. 2014;6:262-74.
32. Gaudino S, Benenati M, Martucci M, Botto A, Infante A, Marrazzo A, et al. Investigating dynamic susceptibility contrast-enhanced perfusion-weighted magnetic resonance imaging in posterior fossa tumors: differences and similarities with supratentorial tumors. Radiol Med. 2020;125(4):416–22.
33. Choi HS, Kim AH, Ahn SS, Shin NY, Kim J, Lee SK. Glioma grading capability: comparisons among parameters from dynamic contrast-enhanced MRI and ADC value on DWI. Korean J Radiol. 2013;14(3):487–92.
34. Arevalo-Perez J, Peck KK, Young RJ, Holodny AI, Karimi S, Lyo JK. Dynamic contrast-enhanced perfusion mri and diffusion-weighted imaging in grading of gliomas. J Neuroimaging. 2015;25(5):792–8.
35. Li X, Zhu Y, Kang H, Zhang Y, Liang H, Wang S, et al. Glioma grading by microvascular permeability parameters derived from dynamic contrast-enhanced MRI and intratumoral susceptibility signal on susceptibility weighted imaging. Cancer Imaging. 2015;15:4.
36. Santarosa C, Castellano A, Conte GM, Cadioli M, Iadanza A, Terreni MR, et al. Dynamic contrast-enhanced and dynamic susceptibility contrast perfusion MR imaging for glioma grading: Preliminary comparison of vessel compartment and permeability parameters using hotspot and histogram analysis. Eur J Radiol. 2016;85(6):1147–56.
37. Jia Z, Geng D, Xie T, Zhang J, Liu Y. Quantitative analysis of neovascular permeability in glioma by dynamic contrast-enhanced MR imaging. J Clin Neurosci. 2012;19(6):820–3.
38. Jung SC, Yeom JA, Kim JH, Ryoo I, Kim SC, Shin H, et al. Glioma: Application of histogram analysis of pharmacokinetic parameters from T1-weighted dynamic contrast-enhanced MR imaging to tumor grading. AJNR Am J Neuroradiol. 2014;35(6):1103–10.
39. Xie T, Chen X, Fang J, Kang H, Xue W, Tong H, et al. Textural features of dynamic contrast-enhanced MRI derived model-free and model-based parameter maps in glioma grading. J Magn Reson Imaging. 2018;47(4):1099–111.
40. Su CQ, Lu SS, Han QY, Zhou MD, Hong XN. Intergrating conventional MRI, texture analysis of dynamic contrast-enhanced MRI, and susceptibility weighted imaging for glioma grading. Acta Radiol. 2019;60(6):777–87.
41. Louis DN, Perry A, Reifenberger G, von Deimling A, Figarella-Branger D, Cavenee WK, et al. The 2016 world health organization classification of tumors of the central nervous system: a summary. Acta Neuropathol. 2016;131(6):803–20.
42. Ahn SS, Shin NY, Chang JH, Kim SH, Kim EH, Kim DW, et al. Prediction of methylguanine methyltransferase promoter methylation in glioblastoma using dynamic contrast-enhanced magnetic resonance and diffusion tensor imaging. J Neurosurg. 2014;121(2):367–73.
43. Di N, Cheng W, Jiang X, Liu X, Zhou J, Xie Q, et al. Can dynamic contrast-enhanced MRI evaluate VEGF expression in brain glioma? An MRI-guided stereotactic biopsy study. J Neuroradiol. 2019;46(3):186–92.
44. Jung BC, Arevalo-Perez J, Lyo JK, Holodny AI, Karimi S, Young RJ, et al. Comparison of glioblastomas and brain metastases using dynamic contrast-enhanced perfusion MRI. J Neuroimaging. 2016;26(2):240–6.
45. Hatzoglou V, Tisnado J, Mehta A, Peck KK, Daras M, Omuro AM, et al. Dynamic contrast-enhanced MRI perfusion for differentiating between melanoma and lung cancer brain metastases. Cancer Med. 2017;6(4):761–7.
46. Zhao J, Yang ZY, Luo BN, Yang JY, Chu JP. Quantitative Evaluation of Diffusion and Dynamic Contrast-Enhanced MR in Tumor Parenchyma and Peritumoral Area for Distinction of Brain Tumors. PLoS One. 2015;10(9):e0138573.
47. Xi YB, Kang XW, Wang N, Liu TT, Zhu YQ, Cheng G, et al. Differentiation of primary central nervous system lymphoma from high-grade glioma and brain metastasis using arterial spin labeling and dynamic contrast-enhanced magnetic resonance imaging. Eur J Radiol. 2019;112:59–64.
48. Toh CH, Wei KC, Chang CN, Ng SH, Wong HF. Differentiation of primary central nervous system lymphomas and glioblastomas: comparisons of diagnostic performance of dynamic susceptibility contrast-enhanced perfusion MR imaging without and with contrast-leakage correction. AJNR Am J Neuroradiol. 2013;34(6):1145–9.
49. Zhang HW, Lyu GW, He WJ, Lei Y, Lin F, Feng YN, et al. Differential diagnosis of central lymphoma and high-grade glioma: dynamic contrast-enhanced histogram. Acta Radiol. 2020;61(9):1221–7.
50. Xu W, Wang Q, Shao A, Xu B, Zhang J. The performance of MR perfusion-weighted imaging for the differentiation of high-grade glioma from primary central nervous system lymphoma: A systematic review and meta-analysis. PLoS One. 2017;12(3):e0173430.
51. Murayama K, Nishiyama Y, Hirose Y, Abe M, Ohyu S, Ninomiya A, et al. Differentiating between central nervous system lymphoma and high-grade glioma using dynamic susceptibility contrast and dynamic contrast-enhanced mr imaging with histogram analysis. Magn Reson Med Sci. 2018;17(1):42–9.
52. Hatzoglou V, Oh JH, Buck O, Lin X, Lee M, Shukla-Dave A, et al. Pretreatment dynamic contrast-enhanced MRI biomarkers correlate with progression-free survival in primary central nervous system lymphoma. J Neurooncol. 2018;140(2):351–8.
53. Fu F, Sun X, Li Y, Liu Y, Shan Y, Ji N, et al. Dynamic contrast-enhanced magnetic resonance imaging biomarkers predict chemotherapeutic responses and survival in primary central-nervous-system lymphoma. Eur Radiol. 2021;31(4):1863–71.

54. van Dijken BRJ, van Laar PJ, Holtman GA, van der Hoorn A. Diagnostic accuracy of magnetic resonance imaging techniques for treatment response evaluation in patients with high-grade glioma, a systematic review and meta-analysis. Eur Radiol. 2017;27(10):4129–44.
55. Morabito R, Alafaci C, Pergolizzi S, Pontoriero A, Iati G, Bonanno L, et al. DCE and DSC perfusion MRI diagnostic accuracy in the follow-up of primary and metastatic intra-axial brain tumors treated by radiosurgery with cyberknife. Radiat Oncol. 2019;14(1):65.
56. Bisdas S, Naegele T, Ritz R, Dimostheni A, Pfannenberg C, Reimold M, et al. Distinguishing recurrent high-grade gliomas from radiation injury: a pilot study using dynamic contrast-enhanced MR imaging. Acad Radiol. 2011;18(5):575–83.
57. Yun TJ, Park CK, Kim TM, Lee SH, Kim JH, Sohn CH, et al. Glioblastoma treated with concurrent radiation therapy and temozolomide chemotherapy: differentiation of true progression from pseudoprogression with quantitative dynamic contrast-enhanced MR imaging. Radiology. 2015;274(3):830–40.
58. Thomas AA, Arevalo-Perez J, Kaley T, Lyo J, Peck KK, Shi W, et al. Dynamic contrast enhanced T1 MRI perfusion differentiates pseudoprogression from recurrent glioblastoma. J Neurooncol. 2015;125(1):183–90.
59. Elshafeey N, Kotrotsou A, Hassan A, Elshafei N, Hassan I, Ahmed S, et al. Multicenter study demonstrates radiomic features derived from magnetic resonance perfusion images identify pseudoprogression in glioblastoma. Nat Commun. 2019;10(1):3170.
60. Nguyen TB, Cron GO, Mercier JF, Foottit C, Torres CH, Chakraborty S, et al. Preoperative prognostic value of dynamic contrast-enhanced MRI-derived contrast transfer coefficient and plasma volume in patients with cerebral gliomas. AJNR Am J Neuroradiol. 2015;36(1):63–9.
61. Kim HS, Kwon SL, Choi SH, Hwang I, Kim TM, Park CK, et al. Prognostication of anaplastic astrocytoma patients: application of contrast leakage information of dynamic susceptibility contrast-enhanced MRI and dynamic contrast-enhanced MRI. Eur Radiol. 2020;30(4):2171–81.
62. Villringer K, Sanz Cuesta BE, Ostwaldt AC, Grittner U, Brunecker P, Khalil AA, et al. DCE-MRI blood-brain barrier assessment in acute ischemic stroke. Neurology. 2017;88(5):433–40.
63. Roh HG, Kim EY, Kim IS, Lee HJ, Park JJ, Lee SB, et al. A Novel collateral imaging method derived from time-resolved dynamic contrast-enhanced MR angiography in acute ischemic stroke: a pilot study. AJNR Am J Neuroradiol. 2019;40(6):946–53.
64. Oh SS, Lee EH, Kim JH, Seo YB, Choo YJ, Park J, et al. The Use of Dynamic Contrast-Enhanced Magnetic Resonance Imaging for the Evaluation of Blood-Brain Barrier Disruption in Traumatic Brain Injury: What Is the Evidence? Brain Sci. 2021;11(6).
65. Lapointe E, Li DKB, Traboulsee AL, Rauscher A. What have we learned from perfusion MRI in multiple sclerosis? AJNR Am J Neuroradiol. 2018;39(6):994–1000.
66. Ingrisch M, Sourbron S, Morhard D, Ertl-Wagner B, Kumpfel T, Hohlfeld R, et al. Quantification of perfusion and permeability in multiple sclerosis: dynamic contrast-enhanced MRI in 3D at 3T. Invest Radiol. 2012;47(4):252–8.
67. Ingrisch M, Sourbron S, Herberich S, Schneider MJ, Kumpfel T, Hohlfeld R, et al. Dynamic contrast-enhanced magnetic resonance imaging suggests normal perfusion in normal-appearing white matter in multiple sclerosis. Invest Radiol. 2017;52(3):135–41.
68. Raja R, Rosenberg GA, Caprihan A. MRI measurements of Blood-Brain Barrier function in dementia: a review of recent studies. Neuropharmacology. 2018;134(Pt B):259–71.
69. van de Haar HJ, Burgmans S, Jansen JF, van Osch MJ, van Buchem MA, Muller M, et al. Blood-brain barrier leakage in patients with early alzheimer disease. Radiology. 2016;281(2):527–35.
70. Kim YS, Kim M, Choi SH, You SH, Yoo RE, Kang KM, et al. Altered vascular permeability in migraine-associated brain regions: evaluation with dynamic contrast-enhanced MRI. Radiology. 2019;292(3):713–20.
71. Lian S, Zhang C, Chi J, Huang Y, Shi F, Xie C. Differentiation between nasopharyngeal carcinoma and lymphoma at the primary site using whole-tumor histogram analysis of apparent diffusion coefficient maps. Radiol Med. 2020;125(7):647–53.
72. Martens RM, Stappen RV, Koopman T, Noij DP, Comans EF, Zwezerijnen GJ, et al. The Additional Value of Ultrafast DCE-MRI to DWI-MRI and 18F-FDG-PET to Detect Occult Primary Head and Neck Squamous Cell Carcinoma. Cancers (Basel). 2020;12(10).
73. Park M, Kim J, Choi YS, Lee SK, Koh YW, Kim SH, et al. Application of dynamic contrast-enhanced mri parameters for differentiating squamous cell carcinoma and malignant lymphoma of the oropharynx. AJR Am J Roentgenol. 2016;206(2):401–7.
74. Pietragalla M, Nardi C, Bonasera L, Mungai F, Taverna C, Novelli L, et al. The role of diffusion-weighted and dynamic contrast enhancement perfusion-weighted imaging in the evaluation of salivary glands neoplasms. Radiol Med. 2020;125(9):851–63.
75. Mungai F, Verrone GB, Bonasera L, Bicci E, Pietragalla M, Nardi C, et al. Imaging biomarkers in the diagnosis of salivary gland tumors: the value of lesion/parenchyma ratio of perfusion-MR pharmacokinetic parameters. Radiol Med. 2021.
76. King AD, Thoeny HC. Functional MRI for the prediction of treatment response in head and neck squamous cell carcinoma: potential and limitations. Cancer Imaging. 2016;16(1):23.
77. Noij DP, de Jong MC, Mulders LG, Marcus JT, de Bree R, Lavini C, et al. Contrast-enhanced perfusion magnetic resonance imaging for head and neck squamous cell carcinoma: a systematic review. Oral Oncol. 2015;51(2):124–38.
78. Ng SH, Lin CY, Chan SC, Lin YC, Yen TC, Liao CT, et al. Clinical utility of multimodality imaging with dynamic contrast-enhanced MRI, diffusion-weighted MRI, and 18F-FDG PET/CT for the prediction of neck control in oropharyngeal or hypopharyngeal squamous cell carcinoma treated with chemoradiation. PLoS One. 2014;9(12):e115933.
79. Chikui T, Kitamoto E, Kawano S, Sugiura T, Obara M, Simonetti AW, et al. Pharmacokinetic analysis based on dynamic contrast-enhanced MRI for evaluating tumor response to preoperative therapy for oral cancer. J Magn Reson Imaging. 2012;36(3):589–97.
80. Wang P, Popovtzer A, Eisbruch A, Cao Y. An approach to identify, from DCE MRI, significant subvolumes of tumors related to outcomes in advanced head-and-neck cancer. Med Phys. 2012;39(8):5277–85.
81. Lee JY, Cheng KL, Lee JH, Choi YJ, Kim HW, Sung YS, et al. Detection of local recurrence in patients with head and neck squamous cell carcinoma using voxel-based color maps of initial and final area under the curve values derived from DCE-MRI. AJNR Am J Neuroradiol. 2019;40(8):1392–401.
82. Fogante M, Tagliati C, De Lisa M, Berardi R, Giuseppetti GM, Giovagnoni A. Correlation between apparent diffusion coefficient of magnetic resonance imaging and tumor-infiltrating lymphocytes in breast cancer. Radiol Med. 2019;124(7):581–7.
83. Travieso-Aja MDM, Maldonado-Saluzzi D, Naranjo-Santana P, Fernandez-Ruiz C, Severino-Rondon W, Rodriguez Rodriguez M, et al. Diagnostic performance of contrast-enhanced dual-energy spectral mammography (CESM): a retrospective study involving 644 breast lesions. Radiol Med. 2019;124(10):1006–17.
84. Amato F, Bicchierai G, Cirone D, Depretto C, Di Naro F, Vanzi E, et al. Preoperative loco-regional staging of invasive lobular

carcinoma with contrast-enhanced digital mammography (CEDM). Radiol Med. 2019;124(12):1229–37.
85. Kuhl CK, Mielcareck P, Klaschik S, Leutner C, Wardelmann E, Gieseke J, et al. Dynamic breast MR imaging: are signal intensity time course data useful for differential diagnosis of enhancing lesions? Radiology. 1999;211(1):101–10.
86. Ahn HS, Jang M, Kim SM, La Yun B, Lee SH. Usefulness of preoperative breast magnetic resonance imaging with a dedicated axillary sequence for the detection of axillary lymph node metastasis in patients with early ductal breast cancer. Radiol Med. 2019;124(12):1220–8.
87. Kinkel K, Helbich TH, Esserman LJ, Barclay J, Schwerin EH, Sickles EA, et al. Dynamic high-spatial-resolution MR imaging of suspicious breast lesions: diagnostic criteria and interobserver variability. AJR Am J Roentgenol. 2000;175(1):35–43.
88. Marino MA, Helbich T, Baltzer P, Pinker-Domenig K. Multiparametric MRI of the breast: a review. J Magn Reson Imaging. 2018;47(2):301–15.
89. Gao Y, Heller SL. Abbreviated and ultrafast breast mri in clinical practice. Radiographics. 2020;40(6):1507–27.
90. Lobbes MB, Prevos R, Smidt M, Tjan-Heijnen VC, van Goethem M, Schipper R, et al. The role of magnetic resonance imaging in assessing residual disease and pathologic complete response in breast cancer patients receiving neoadjuvant chemotherapy: a systematic review. Insights Imaging. 2013;4(2):163–75.
91. Marinovich ML, Houssami N, Macaskill P, Sardanelli F, Irwig L, Mamounas EP, et al. Meta-analysis of magnetic resonance imaging in detecting residual breast cancer after neoadjuvant therapy. J Natl Cancer Inst. 2013;105(5):321–33.
92. Fowler AM, Mankoff DA, Joe BN. Imaging neoadjuvant therapy response in breast cancer. Radiology. 2017;285(2):358–75.
93. Ah-See ML, Makris A, Taylor NJ, Harrison M, Richman PI, Burcombe RJ, et al. Early changes in functional dynamic magnetic resonance imaging predict for pathologic response to neoadjuvant chemotherapy in primary breast cancer. Clin Cancer Res. 2008;14(20):6580–9.
94. Dogan BE, Yuan Q, Bassett R, Guvenc I, Jackson EF, Cristofanilli M, et al. Comparing the performances of magnetic resonance imaging size vs pharmacokinetic parameters to predict response to neoadjuvant chemotherapy and survival in patients with breast cancer. Curr Probl Diagn Radiol. 2019;48(3):235–40.
95. Mann RM, Balleyguier C, Baltzer PA, Bick U, Colin C, Cornford E, et al. Breast MRI: EUSOBI recommendations for women's information. Eur Radiol. 2015;25(12):3669–78.
96. Chapman MC, Hayward JH, Woodard GA, Joe BN, Lee AY. The role of breast MRI in detecting asymptomatic recurrence after therapeutic mastectomy. AJR Am J Roentgenol. 2020;215(1):254–61.
97. Drew PJ, Kerin MJ, Turnbull LW, Imrie M, Carleton PJ, Fox JN, et al. Routine screening for local recurrence following breast-conserving therapy for cancer with dynamic contrast-enhanced magnetic resonance imaging of the breast. Ann Surg Oncol. 1998;5(3):265–70.
98. Preda L, Villa G, Rizzo S, Bazzi L, Origgi D, Cassano E, et al. Magnetic resonance mammography in the evaluation of recurrence at the prior lumpectomy site after conservative surgery and radiotherapy. Breast Cancer Res. 2006;8(5):R53.
99. Mirsadraee S, van Beek EJ. Functional imaging: computed tomography and MRI. Clin Chest Med. 2015;36(2):349-63, x.
100. Ohno Y, Fujisawa Y, Yui M, Takenaka D, Koyama H, Sugihara N, et al. Solitary pulmonary nodule: Comparison of quantitative capability for differentiation and management among dynamic CE-perfusion MRI at 3T system, dynamic CE-perfusion ADCT and FDG-PET/CT. Eur J Radiol. 2019;115:22–30.
101. Contegiacomo A, Del Ciello A, Rella R, Attempati N, Coppolino D, Larici AR, et al. Pulmonary arteriovenous malformations: what the interventional radiologist needs to know. Radiol Med. 2019;124(10):973–88.
102. Agostini A, Borgheresi A, Mari A, Floridi C, Bruno F, Carotti M, et al. Dual-energy CT: theoretical principles and clinical applications. Radiol Med. 2019;124(12):1281–95.
103. Ohno Y, Koyama H, Lee HY, Miura S, Yoshikawa T, Sugimura K. Contrast-enhanced CT- and MRI-based perfusion assessment for pulmonary diseases: basics and clinical applications. Diagn Interv Radiol. 2016;22(5):407–21.
104. Aziz M, Krishnam M, Madhuranthakam AJ, Rajiah P. Update on MR imaging of the pulmonary vasculature. Int J Cardiovasc Imaging. 2019;35(8):1483–97.
105. Ohno Y, Yoshikawa T, Kishida Y, Seki S, Karabulut N. Unenhanced and contrast-enhanced MR angiography and perfusion imaging for suspected pulmonary thromboembolism. AJR Am J Roentgenol. 2017;208(3):517–30.
106. Johns CS, Swift AJ, Hughes PJC, Ohno Y, Schiebler M, Wild JM. Pulmonary MR angiography and perfusion imaging-A review of methods and applications. Eur J Radiol. 2017;86:361–70.
107. Moher Alsady T, Kaireit TF, Behrendt L, Winther HB, Olsson KM, Wacker F, et al. Comparison of dual-energy computer tomography and dynamic contrast-enhanced MRI for evaluating lung perfusion defects in chronic thromboembolic pulmonary hypertension. PLoS One. 2021;16(6):e0251740.
108. Ohno Y, Nishio M, Koyama H, Miura S, Yoshikawa T, Matsumoto S, et al. Dynamic contrast-enhanced CT and MRI for pulmonary nodule assessment. AJR Am J Roentgenol. 2014;202(3):515–29.
109. Wang J, Wu N, Cham MD, Song Y. Tumor response in patients with advanced non-small cell lung cancer: perfusion CT evaluation of chemotherapy and radiation therapy. AJR Am J Roentgenol. 2009;193(4):1090–6.
110. Ohno Y, Nogami M, Higashino T, Takenaka D, Matsumoto S, Hatabu H, et al. Prognostic value of dynamic MR imaging for non-small-cell lung cancer patients after chemoradiotherapy. J Magn Reson Imaging. 2005;21(6):775–83.
111. Hecht EM, Rosenkrantz A. Pulmonary MR angiography techniques and applications. Magn Reson Imaging Clin N Am. 2009;17(1):101–31.
112. Kluge A, Luboldt W, Bachmann G. Acute pulmonary embolism to the subsegmental level: diagnostic accuracy of three MRI techniques compared with 16-MDCT. AJR Am J Roentgenol. 2006;187(1):W7-14.
113. Tonino PA, De Bruyne B, Pijls NH, Siebert U, Ikeno F, van' t Veer M, et al. Fractional flow reserve versus angiography for guiding percutaneous coronary intervention. N Engl J Med. 2009;360(3):213-24.
114. Pierpaolo P, Rolf S, Manuel BP, Davide C, Dresselaers T, Claus P, et al. Left ventricular global myocardial strain assessment: Are CMR feature-tracking algorithms useful in the clinical setting? Radiol Med. 2020;125(5):444–50.
115. Pradella S, Grazzini G, De Amicis C, Letteriello M, Acquafresca M, Miele V. Cardiac magnetic resonance in hypertrophic and dilated cardiomyopathies. Radiol Med. 2020;125(11):1056–71.
116. Palumbo P, Cannizzaro E, Di Cesare A, Bruno F, Schicchi N, Giovagnoni A, et al. Cardiac magnetic resonance in arrhythmogenic cardiomyopathies. Radiol Med. 2020;125(11):1087–101.
117. Palmisano A, Vignale D, Benedetti G, Del Maschio A, De Cobelli F, Esposito A. Late iodine enhancement cardiac computed tomography for detection of myocardial scars:

impact of experience in the clinical practice. Radiol Med. 2020;125(2):128–36.
118. Agliata G, Schicchi N, Agostini A, Fogante M, Mari A, Maggi S, et al. Radiation exposure related to cardiovascular CT examination: comparison between conventional 64-MDCT and third-generation dual-source MDCT. Radiol Med. 2019;124(8):753–61.
119. De Rubeis G, Marchitelli L, Spano G, Catapano F, Cilia F, Galea N, et al. Radiological outpatient' visits to avoid inappropriate cardiac CT examinations: an 8-year experience report. Radiol Med. 2021;126(2):214–20.
120. Seker M. Prevalence and morphologic features of dual left anterior descending artery subtypes in coronary CT angiography. Radiol Med. 2020;125(3):247–56.
121. Takehara Y. 4D Flow when and how? Radiol Med. 2020;125(9):838–50.
122. Marano R, Rovere G, Savino G, Flammia FC, Carafa MRP, Steri L, et al. CCTA in the diagnosis of coronary artery disease. Radiol Med. 2020;125(11):1102–13.
123. Ippolito D, Riva L, Talei Franzesi CR, Cangiotti C, De Vito A, Di Gennaro F, et al. Diagnostic efficacy of model-based iterative reconstruction algorithm in an assessment of coronary artery in comparison with standard hybrid-Iterative reconstruction algorithm: dose reduction and image quality. Radiol Med. 2019;124(5):350–9.
124. Liguori C, Farina D, Vaccher F, Ferrandino G, Bellini D, Carbone I. Myocarditis: imaging up to date. Radiol Med. 2020;125(11):1124–34.
125. Alitto AR, Chiesa S, Franco P, Fiore M, Marino L, Borghetti P, et al. PAIDEIA: pacemaker and implanted cardioverter defibrillator management in radiation therapy-a survey by the Young Group of the Italian Association of Radiotherapy and Clinical Oncology (AIRO). Radiol Med. 2020;125(3):329–35.
126. Galea N, Polizzi G, Gatti M, Cundari G, Figuera M, Faletti R. Cardiovascular magnetic resonance (CMR) in restrictive cardiomyopathies. Radiol Med. 2020;125(11):1072–86.
127. Ciancarella P, Ciliberti P, Santangelo TP, Secchi F, Stagnaro N, Secinaro A. Noninvasive imaging of congenital cardiovascular defects. Radiol Med. 2020;125(11):1167–85.
128. Daghighi S, Chan A, Kiani Nazarlou A, Hasan Z, Halimi M, Akbarzadeh F, et al. Clinical and histopathological outcome of cervical and chest MRI involving non-MRI-conditional cardiac pacemakers: a study using sheep models. Radiol Med. 2020;125(8):706–14.
129. La Grutta L, Toia P, Grassedonio E, Pasta S, Albano D, Agnello F, et al. TAVI imaging: over the echocardiography. Radiol Med. 2020;125(11):1148–66.
130. Valente T, Pignatiello M, Sica G, Bocchini G, Rea G, Cappabianca S, et al. Hemopericardium in the acute clinical setting: Are we ready for a tailored management approach on the basis of MDCT findings? Radiol Med. 2020.
131. Guerrini L, Mazzocchi S, Giomi A, Milli M, Carpi R. An operational approach to the execution of MR examinations in patients with CIED. Radiol Med. 2020;125(12):1311–21.
132. van Assen M, Muscogiuri G, Caruso D, Lee SJ, Laghi A, De Cecco CN. Artificial intelligence in cardiac radiology. Radiol Med. 2020;125(11):1186–99.
133. Buffa V, Di Renzi P. CMR in the diagnosis of ischemic heart disease. Radiol Med. 2020;125(11):1114–23.
134. Centonze M, Steidler S, Casagranda G, Alfonsi U, Spagnolli F, Rozzanigo U, et al. Cardiac-CT and cardiac-MR cost-effectiveness: a literature review. Radiol Med. 2020;125(11):1200–7.
135. Di Cesare E, Carerj S, Palmisano A, Carerj ML, Catapano F, Vignale D, et al. Multimodality imaging in chronic heart failure. Radiol Med. 2021;126(2):231–42.
136. Li M, Zhou T, Yang LF, Peng ZH, Ding J, Sun G. Diagnostic accuracy of myocardial magnetic resonance perfusion to diagnose ischemic stenosis with fractional flow reserve as reference: systematic review and meta-analysis. JACC Cardiovasc Imaging. 2014;7(11):1098–105.
137. Rovere G, Meduri A, Savino G, Flammia FC, Lo Piccolo F, Carafa MRP, et al. Practical instructions for using drugs in CT and MR cardiac imaging. Radiol Med. 2021;126(3):356–64.
138. Seitun S, Clemente A, Maffei E, Toia P, La Grutta L, Cademartiri F. Prognostic value of cardiac CT. Radiol Med. 2020;125(11):1135–47.
139. Esposito A, Gallone G, Palmisano A, Marchitelli L, Catapano F, Francone M. The current landscape of imaging recommendations in cardiovascular clinical guidelines: toward an imaging-guided precision medicine. Radiol Med. 2020;125(11):1013–23.
140. Palumbo P, Cannizzaro E, Bruno F, Schicchi N, Fogante M, Agostini A, et al. Coronary artery disease (CAD) extension-derived risk stratification for asymptomatic diabetic patients: usefulness of low-dose coronary computed tomography angiography (CCTA) in detecting high-risk profile patients. Radiol Med. 2020;125(12):1249–59.
141. Pelgrim GJ, Handayani A, Dijkstra H, Prakken NH, Slart RH, Oudkerk M, et al. Quantitative Myocardial Perfusion with Dynamic Contrast-Enhanced Imaging in MRI and CT: Theoretical Models and Current Implementation. Biomed Res Int. 2016;2016:1734190.
142. van Assen M, Muscogiuri G, Caruso D, Lee SJ, Laghi A, De Cecco CN. Artificial intelligence in cardiac radiology. La radiologia medica. 2020;125(11):1186–99.
143. Russo V, Lovato L, Ligabue G. Cardiac MRI: technical basis. Radiol Med. 2020;125(11):1040–55.
144. Nagel E, Greenwood JP, McCann GP, Bettencourt N, Shah AM, Hussain ST, et al. Magnetic resonance perfusion or fractional flow reserve in coronary disease. N Engl J Med. 2019;380(25):2418–28.
145. Marcos-Garces V, Gavara J, Monmeneu JV, Lopez-Lereu MP, Bosch MJ, Merlos P, et al. Vasodilator stress CMR and all-cause mortality in stable ischemic heart disease: a large retrospective registry. JACC Cardiovasc Imaging. 2020;13(8):1674–86.
146. Sammut EC, Villa ADM, Di Giovine G, Dancy L, Bosio F, Gibbs T, et al. Prognostic value of quantitative stress perfusion cardiac magnetic resonance. JACC Cardiovasc Imaging. 2018;11(5):686–94.
147. Schicchi N, Fogante M, Esposto Pirani P, Agliata G, Basile MC, Oliva M, et al. Third-generation dual-source dual-energy CT in pediatric congenital heart disease patients: state-of-the-art. Radiol Med. 2019;124(12):1238–52.
148. Schicchi N, Mari A, Fogante M, Esposto Pirani P, Agliata G, Tosi N, et al. In vivo radiation dosimetry and image quality of turboflash and retrospective dual-source CT coronary angiography. Radiol Med. 2020;125(2):117–27.
149. Tanabe Y, Kurata A, Matsuda T, Yoshida K, Baruah D, Kido T, et al. Computed tomographic evaluation of myocardial ischemia. Jpn J Radiol. 2020;38(5):411–33.
150. Takx RA, Blomberg BA, El Aidi H, Habets J, de Jong PA, Nagel E, et al. Diagnostic accuracy of stress myocardial perfusion imaging compared to invasive coronary angiography with fractional flow reserve meta-analysis. Circ Cardiovasc Imaging. 2015;8(1).
151. Chen MY, Rochitte CE, Arbab-Zadeh A, Dewey M, George RT, Miller JM, et al. Prognostic value of combined CT angiography and myocardial perfusion imaging versus invasive coronary angiography and nuclear stress perfusion imaging in the prediction of major adverse cardiovascular events: the CORE320 multicenter study. Radiology. 2017;284(1):55–65.

152. Grandhi GR, Batlle JC, Maroules CD, Janowitz W, Pena CS, Ziffer JA, et al. Combined stress myocardial CT perfusion and coronary CT angiography as a feasible strategy among patients presenting with acute chest pain to the emergency department. J Cardiovasc Comput Tomogr. 2021;15(2):129–36.
153. Sahani DV, Holalkere NS, Mueller PR, Zhu AX. Advanced hepatocellular carcinoma: CT perfusion of liver and tumor tissue–initial experience. Radiology. 2007;243(3):736–43.
154. Hu HT, Shan QY, Chen SL, Li B, Feng ST, Xu EJ, et al. CT-based radiomics for preoperative prediction of early recurrent hepatocellular carcinoma: technical reproducibility of acquisition and scanners. Radiol Med. 2020;125(8):697–705.
155. Miles KA, Lee TY, Goh V, Klotz E, Cuenod C, Bisdas S, et al. Current status and guidelines for the assessment of tumour vascular support with dynamic contrast-enhanced computed tomography. Eur Radiol. 2012;22(7):1430–41.
156. Miles KA. Perfusion CT for the assessment of tumour vascularity: which protocol? Br J Radiol. 2003;76 Spec No 1:S36-42.
157. Yoon JH, Lee JM, Yu MH, Hur BY, Grimm R, Sourbron S, et al. Simultaneous evaluation of perfusion and morphology using GRASP MRI in hepatic fibrosis. Eur Radiol. 2021.
158. Kajita K, Goshima S, Noda Y, Kawada H, Kawai N, Okuaki T, et al. Thin-slice free-breathing pseudo-golden-angle radial stack-of-stars with gating and tracking T1-weighted acquisition: an efficient gadoxetic acid-enhanced hepatobiliary-phase imaging alternative for patients with unstable breath holding. Magn Reson Med Sci. 2019;18(1):4–11.
159. Blomley MJ, Coulden R, Dawson P, Kormano M, Donlan P, Bufkin C, et al. Liver perfusion studied with ultrafast CT. J Comput Assist Tomogr. 1995;19(3):424–33.
160. Miles KA, Charnsangavej C, Lee FT, Fishman EK, Horton K, Lee TY. Application of CT in the investigation of angiogenesis in oncology. Acad Radiol. 2000;7(10):840–50.
161. Ng CS, Chandler AG, Wei W, Anderson EF, Herron DH, Kurzrock R, et al. Effect of dual vascular input functions on CT perfusion parameter values and reproducibility in liver tumors and normal liver. J Comput Assist Tomogr. 2012;36(4):388–93.
162. Petralia G, Bonello L, Viotti S, Preda L, d'Andrea G, Bellomi M. CT perfusion in oncology: how to do it. Cancer Imaging. 2010;10:8–19.
163. Bottari A, Silipigni S, Carerj ML, Cattafi A, Maimone S, Marino MA, et al. Dual-source dual-energy CT in the evaluation of hepatic fractional extracellular space in cirrhosis. Radiol Med. 2020;125(1):7–14.
164. Mathew RP, Sam M, Raubenheimer M, Patel V, Low G. Hepatic hemangiomas: the various imaging avatars and its mimickers. Radiol Med. 2020;125(9):801–15.
165. Shin N, Choi JA, Choi JM, Cho ES, Kim JH, Chung JJ, et al. Sclerotic changes of cavernous hemangioma in the cirrhotic liver: long-term follow-up using dynamic contrast-enhanced computed tomography. Radiol Med. 2020;125(12):1225–32.
166. Kim KW, Lee JM, Klotz E, Park HS, Lee DH, Kim JY, et al. Quantitative CT color mapping of the arterial enhancement fraction of the liver to detect hepatocellular carcinoma. Radiology. 2009;250(2):425–34.
167. Li JP, Feng GL, Li DQ, Wang HB, Zhao DL, Wan Y, et al. Detection and differentiation of early hepatocellular carcinoma from cirrhosis using CT perfusion in a rat liver model. Hepatobiliary Pancreat Dis Int. 2016;15(6):612–8.
168. Calandri M, Ruggeri V, Carucci P, Mirabella S, Veltri A, Fonio P, et al. Thermal ablation with fusion imaging guidance of hepatocellular carcinoma without conspicuity on conventional or contrast-enhanced US: surrounding anatomical landmarks matter. Radiol Med. 2019;124(10):1043–8.
169. Esposito A, Buscarino V, Raciti D, Casiraghi E, Manini M, Biondetti P, et al. Characterization of liver nodules in patients with chronic liver disease by MRI: performance of the Liver Imaging Reporting and Data System (LI-RADS vol 2018) scale and its comparison with the Likert scale. Radiol Med. 2020;125(1):15–23.
170. Gatti M, Calandri M, Bergamasco L, Darvizeh F, Grazioli L, Inchingolo R, et al. Characterization of the arterial enhancement pattern of focal liver lesions by multiple arterial phase magnetic resonance imaging: comparison between hepatocellular carcinoma and focal nodular hyperplasia. Radiol Med. 2020;125(4):348–55.
171. Tsushima Y, Blomley MJ, Yokoyama H, Kusano S, Endo K. Does the presence of distant and local malignancy alter parenchymal perfusion in apparently disease-free areas of the liver? Dig Dis Sci. 2001;46(10):2113–9.
172. Ippolito D, Pecorelli A, Querques G, Drago SG, Maino C, Franzesi CT, et al. Dynamic computed tomography perfusion imaging: complementary diagnostic tool in hepatocellular carcinoma assessment from diagnosis to treatment follow-up. Acad Radiol. 2019;26(12):1675–85.
173. Borgheresi A, Gonzalez-Aguirre A, Brown KT, Getrajdman GI, Erinjeri JP, Covey A, et al. Does enhancement or perfusion on preprocedure CT predict outcomes after embolization of hepatocellular carcinoma? Acad Radiol. 2018;25(12):1588–94.
174. Miles KA, Leggett DA, Kelley BB, Hayball MP, Sinnatamby R, Bunce I. In vivo assessment of neovascularization of liver metastases using perfusion CT. Br J Radiol. 1998;71(843):276–81.
175. Kim DH, Kim SH, Im SA, Han SW, Goo JM, Willmann JK, et al. Intermodality comparison between 3D perfusion CT and 18F-FDG PET/CT imaging for predicting early tumor response in patients with liver metastasis after chemotherapy: preliminary results of a prospective study. Eur J Radiol. 2012;81(11):3542–50.
176. Ng CS, Charnsangavej C, Wei W, Yao JC. Perfusion CT findings in patients with metastatic carcinoid tumors undergoing bevacizumab and interferon therapy. AJR Am J Roentgenol. 2011;196(3):569–76.
177. Ravanelli M, Agazzi GM, Tononcelli E, Roca E, Cabassa P, Baiocchi G, et al. Texture features of colorectal liver metastases on pretreatment contrast-enhanced CT may predict response and prognosis in patients treated with bevacizumab-containing chemotherapy: a pilot study including comparison with standard chemotherapy. Radiol Med. 2019;124(9):877–86.
178. Mahnken AH, Klotz E, Schreiber S, Bruners P, Isfort P, Gunther RW, et al. Volumetric arterial enhancement fraction predicts tumor recurrence after hepatic radiofrequency ablation of liver metastases: initial results. AJR Am J Roentgenol. 2011;196(5):W573-9.
179. Miles KA, Hayball MP, Dixon AK. Functional images of hepatic perfusion obtained with dynamic CT. Radiology. 1993;188(2):405–11.
180. Hagiwara M, Rusinek H, Lee VS, Losada M, Bannan MA, Krinsky GA, et al. Advanced liver fibrosis: diagnosis with 3D whole-liver perfusion MR imaging–initial experience. Radiology. 2008;246(3):926–34.
181. Cappabianca S, Iaselli F, Reginelli A, D'Andrea A, Urraro F, Grassi R, et al. Value of diffusion-weighted magnetic resonance imaging in the characterization of complex adnexal masses. Tumori. 2013;99(2):210–7.
182. Cuenod CA, Fournier L, Balvay D, Guinebretiere JM. Tumor angiogenesis: pathophysiology and implications for contrast-enhanced MRI and CT assessment. Abdom Imaging. 2006;31(2):188–93.
183. Iacobellis F, Berritto D, Somma F, Cavaliere C, Corona M, Cozzolino S, et al. Magnetic resonance imaging: a new tool

for diagnosis of acute ischemic colitis? World J Gastroenterol. 2012;18(13):1496–501.
184. Pellino G, Gallo G, Pallante P, Capasso R, De Stefano A, Maretto I, et al. Noninvasive biomarkers of colorectal cancer: role in diagnosis and personalised treatment perspectives. Gastroenterol Res Pract. 2018;2018:2397863.
185. Reginelli A, Mandato Y, Solazzo A, Berritto D, Iacobellis F, Grassi R. Errors in the radiological evaluation of the alimentary tract: part II. Semin Ultrasound CT MR. 2012;33(4):308–17.
186. Somma F, Faggian A, Serra N, Gatta G, Iacobellis F, Berritto D, et al. Bowel intussusceptions in adults: the role of imaging. Radiol Med. 2015;120(1):105–17.
187. Belfiore G, Belfiore MP, Reginelli A, Capasso R, Romano F, Ianniello GP, et al. Concurrent chemotherapy alone versus irreversible electroporation followed by chemotherapy on survival in patients with locally advanced pancreatic cancer. Med Oncol. 2017;34(3):38.
188. Scialpi M, Reginelli A, D'Andrea A, Gravante S, Falcone G, Baccari P, et al. Pancreatic tumors imaging: An update. Int J Surg. 2016;28(Suppl 1):S142-55.
189. Hu R, Yang H, Chen Y, Zhou T, Zhang J, Chen TW, et al. Dynamic contrast-enhanced mri for measuring pancreatic perfusion in acute pancreatitis: a preliminary study. Acad Radiol. 2019;26(12):1641–9.
190. Eriksen RO, Strauch LS, Sandgaard M, Kristensen TS, Nielsen MB, Lauridsen CA. Dynamic Contrast-Enhanced CT in Patients with Pancreatic Cancer. Diagnostics (Basel). 2016;6(3).
191. Reginelli A, Vanzulli A, Sgrazzutti C, Caschera L, Serra N, Raucci A, et al. Vascular microinvasion from hepatocellular carcinoma: CT findings and pathologic correlation for the best therapeutic strategies. Med Oncol. 2017;34(5):93.
192. Scialpi M, Palumbo B, Pierotti L, Gravante S, Piunno A, Rebonato A, et al. Detection and characterization of focal liver lesions by split-bolus multidetector-row CT: diagnostic accuracy and radiation dose in oncologic patients. Anticancer Res. 2014;34(8):4335–44.
193. Kandel S, Kloeters C, Meyer H, Hein P, Hilbig A, Rogalla P. Whole-organ perfusion of the pancreas using dynamic volume CT in patients with primary pancreas carcinoma: acquisition technique, post-processing and initial results. Eur Radiol. 2009;19(11):2641–6.
194. Oostendorp M, Post MJ, Backes WH. Vessel growth and function: depiction with contrast-enhanced MR imaging. Radiology. 2009;251(2):317–35.
195. Motosugi U, Ichikawa T, Morisaka H, Sou H, Muhi A, Kimura K, et al. Detection of pancreatic carcinoma and liver metastases with gadoxetic acid-enhanced MR imaging: comparison with contrast-enhanced multi-detector row CT. Radiology. 2011;260(2):446–53.
196. Granata V, Fusco R, Sansone M, Grassi R, Maio F, Palaia R, et al. Magnetic resonance imaging in the assessment of pancreatic cancer with quantitative parameter extraction by means of dynamic contrast-enhanced magnetic resonance imaging, diffusion kurtosis imaging and intravoxel incoherent motion diffusion-weighted imaging. Therap Adv Gastroenterol. 2020;13:1756284819885052.
197. Srisajjakul S, Prapaisilp P, Bangchokdee S. CT and MR features that can help to differentiate between focal chronic pancreatitis and pancreatic cancer. Radiol Med. 2020;125(4):356–64.
198. Bali MA, Metens T, Denolin V, Delhaye M, Demetter P, Closset J, et al. Tumoral and nontumoral pancreas: correlation between quantitative dynamic contrast-enhanced MR imaging and histopathologic parameters. Radiology. 2011;261(2):456–66.
199. Coenegrachts K, Van Steenbergen W, De Keyzer F, Vanbeckevoort D, Bielen D, Chen F, et al. Dynamic contrast-enhanced MRI of the pancreas: initial results in healthy volunteers and patients with chronic pancreatitis. J Magn Reson Imaging. 2004;20(6):990–7.
200. Zhang XM, Shi H, Parker L, Dohke M, Holland GA, Mitchell DG. Suspected early or mild chronic pancreatitis: enhancement patterns on gadolinium chelate dynamic MRI. Magnetic resonance imaging. J Magn Reson Imaging. 2003;17(1):86-94.
201. Akisik MF, Sandrasegaran K, Bu G, Lin C, Hutchins GD, Chiorean EG. Pancreatic cancer: utility of dynamic contrast-enhanced MR imaging in assessment of antiangiogenic therapy. Radiology. 2010;256(2):441–9.
202. Grazzini G, Danti G, Cozzi D, Lanzetta MM, Addeo G, Falchini M, et al. Diagnostic imaging of gastrointestinal neuroendocrine tumours (GI-NETs): relationship between MDCT features and 2010 WHO classification. Radiol Med. 2019;124(2):94–102.
203. Joo I, Lee JM, Han JK, Yang HK, Lee HJ, Choi BI. Dynamic contrast-enhanced MRI of gastric cancer: Correlation of the perfusion parameters with pathological prognostic factors. J Magn Reson Imaging. 2015;41(6):1608–14.
204. Ma L, Xu X, Zhang M, Zheng S, Zhang B, Zhang W, et al. Dynamic contrast-enhanced MRI of gastric cancer: Correlations of the pharmacokinetic parameters with histological type, Lauren classification, and angiogenesis. Magn Reson Imaging. 2017;37:27–32.
205. Tang L, Wang XJ, Baba H, Giganti F. Gastric cancer and image-derived quantitative parameters: Part 2-a critical review of DCE-MRI and (18)F-FDG PET/CT findings. Eur Radiol. 2020;30(1):247–60.
206. Zhu YJ, Li Y, Jiang J, Zhang W, Xue LY, Zhou AP, et al. Predictive value of quantitative dynamic contrast-enhanced magnetic resonance imaging for the efficacy of neoadjuvant chemotherapy in locally advanced gastric cancer. Zhonghua Zhong Liu Za Zhi. 2019;41(10):765–70.
207. Correale P, Botta C, Staropoli N, Nardone V, Pastina P, Ulivieri C, et al. Systemic inflammatory status predict the outcome of k-RAS WT metastatic colorectal cancer patients receiving the thymidylate synthase poly-epitope-peptide anticancer vaccine. Oncotarget. 2018;9(29):20539–54.
208. Zhu Y, Zhou Y, Zhang W, Xue L, Li Y, Jiang J, et al. Value of quantitative dynamic contrast-enhanced and diffusion-weighted magnetic resonance imaging in predicting extramural venous invasion in locally advanced gastric cancer and prognostic significance. Quant Imaging Med Surg. 2021;11(1):328–40.
209. Intven M, Reerink O, Philippens ME. Dynamic contrast enhanced MR imaging for rectal cancer response assessment after neo-adjuvant chemoradiation. J Magn Reson Imaging. 2015;41(6):1646–53.
210. Petrillo A, Fusco R, Petrillo M, Granata V, Sansone M, Avallone A, et al. Standardized Index of Shape (SIS): a quantitative DCE-MRI parameter to discriminate responders by non-responders after neoadjuvant therapy in LARC. Eur Radiol. 2015;25(7):1935–45.
211. Petrillo M, Fusco R, Catalano O, Sansone M, Avallone A, Delrio P, et al. MRI for Assessing Response to Neoadjuvant Therapy in Locally Advanced Rectal Cancer Using DCE-MR and DW-MR Data Sets: A Preliminary Report. Biomed Res Int. 2015;2015:514740.
212. Fornell-Perez R, Vivas-Escalona V, Aranda-Sanchez J, Gonzalez-Dominguez MC, Rubio-Garcia J, Aleman-Flores P, et al. Primary and post-chemoradiotherapy MRI detection of extramural venous invasion in rectal cancer: the role of diffusion-weighted imaging. Radiol Med. 2020;125(6):522–30.
213. Ciolina M, Caruso D, De Santis D, Zerunian M, Rengo M, Alfieri N, et al. Dynamic contrast-enhanced magnetic resonance imaging in locally advanced rectal cancer: role of perfusion

parameters in the assessment of response to treatment. Radiol Med. 2019;124(5):331–8.
214. Kim SH, Lee JM, Gupta SN, Han JK, Choi BI. Dynamic contrast-enhanced MRI to evaluate the therapeutic response to neoadjuvant chemoradiation therapy in locally advanced rectal cancer. J Magn Reson Imaging. 2014;40(3):730–7.
215. Tong T, Sun Y, Gollub MJ, Peng W, Cai S, Zhang Z, et al. Dynamic contrast-enhanced MRI: Use in predicting pathological complete response to neoadjuvant chemoradiation in locally advanced rectal cancer. J Magn Reson Imaging. 2015;42(3):673–80.
216. Boldrini L, Cusumano D, Chiloiro G, Casa C, Masciocchi C, Lenkowicz J, et al. Delta radiomics for rectal cancer response prediction with hybrid 0.35 T magnetic resonance-guided radiotherapy (MRgRT): a hypothesis-generating study for an innovative personalized medicine approach. Radiol Med. 2019;124(2):145-53.
217. Armbruster M, D'Anastasi M, Holzner V, Kreis ME, Dietrich O, Brandlhuber B, et al. Improved detection of a tumorous involvement of the mesorectal fascia and locoregional lymph nodes in locally advanced rectal cancer using DCE-MRI. Int J Colorectal Dis. 2018;33(7):901–9.
218. Kim YE, Lim JS, Choi J, Kim D, Myoung S, Kim MJ, et al. Perfusion parameters of dynamic contrast-enhanced magnetic resonance imaging in patients with rectal cancer: correlation with microvascular density and vascular endothelial growth factor expression. Korean J Radiol. 2013;14(6):878–85.
219. Lollert A, Junginger T, Schimanski CC, Biesterfeld S, Gockel I, Duber C, et al. Rectal cancer: dynamic contrast-enhanced MRI correlates with lymph node status and epidermal growth factor receptor expression. J Magn Reson Imaging. 2014;39(6):1436–42.
220. Shen FU, Lu J, Chen L, Wang Z, Chen Y. Diagnostic value of dynamic contrast-enhanced magnetic resonance imaging in rectal cancer and its correlation with tumor differentiation. Mol Clin Oncol. 2016;4(4):500–6.
221. Yao WW, Zhang H, Ding B, Fu T, Jia H, Pang L, et al. Rectal cancer: 3D dynamic contrast-enhanced MRI; correlation with microvascular density and clinicopathological features. Radiol Med. 2011;116(3):366–74.
222. Yeo DM, Oh SN, Jung CK, Lee MA, Oh ST, Rha SE, et al. Correlation of dynamic contrast-enhanced MRI perfusion parameters with angiogenesis and biologic aggressiveness of rectal cancer: Preliminary results. J Magn Reson Imaging. 2015;41(2):474–80.
223. Lassau N, Chami L, Koscielny S, Chebil M, Massard C, Benatsou B, et al. Quantitative functional imaging by dynamic contrast enhanced ultrasonography (DCE-US) in GIST patients treated with masatinib. Invest New Drugs. 2012;30(2):765–71.
224. Brillantino A, Iacobellis F, Reginelli A, Monaco L, Sodano B, Tufano G, et al. Preoperative assessment of simple and complex anorectal fistulas: Tridimensional endoanal ultrasound? Magnetic resonance? Both? Radiol Med. 2019;124(5):339–49.
225. Masselli G, De Vincentiis C, Aloi M, Guida M, Cao R, Cartocci G, et al. Detection of Crohn's disease with diffusion images versus contrast-enhanced images in pediatric using MR enterography with histopathological correlation. Radiol Med. 2019;124(12):1306–14.
226. Vieujean S, Coibion C, Seidel L, Louis E, Meunier P. Magnetic resonance enterography perfusion parameters reveal complex changes in affected and unaffected segments in Crohn's disease. Scand J Gastroenterol. 2020;55(9):1041–8.
227. Wu YC, Xiao ZB, Lin XH, Zheng XY, Cao DR, Zhang ZS. Dynamic contrast-enhanced magnetic resonance imaging and diffusion-weighted imaging in the activity staging of terminal ileum Crohn's disease. World J Gastroenterol. 2020;26(39):6057–73.
228. Del Vescovo R, Pisanti F, Russo V, Battisti S, Cazzato RL, D'Agostino F, et al. Dynamic contrast-enhanced MR evaluation of prostate cancer before and after endorectal high-intensity focused ultrasound. Radiol Med. 2013;118(5):851–62.
229. Lee S, Choi YH, Cho YJ, Cheon JE, Moon JS, Kang GH, et al. Quantitative evaluation of Crohn's disease using dynamic contrast-enhanced MRI in children and young adults. Eur Radiol. 2020;30(6):3168–77.
230. Florie J, Wasser MN, Arts-Cieslik K, Akkerman EM, Siersema PD, Stoker J. Dynamic contrast-enhanced MRI of the bowel wall for assessment of disease activity in Crohn's disease. AJR Am J Roentgenol. 2006;186(5):1384–92.
231. Bhatnagar G, Dikaios N, Prezzi D, Vega R, Halligan S, Taylor SA. Changes in dynamic contrast-enhanced pharmacokinetic and diffusion-weighted imaging parameters reflect response to anti-TNF therapy in Crohn's disease. Br J Radiol. 2015;88(1055):20150547.
232. Zhu J, Zhang F, Zhou J, Li H. Assessment of therapeutic response in Crohn's disease using quantitative dynamic contrast enhanced MRI (DCE-MRI) parameters: A preliminary study. Medicine (Baltimore). 2017;96(32):e7759.
233. Saevik F, Nylund K, Hausken T, Odegaard S, Gilja OH. Bowel perfusion measured with dynamic contrast-enhanced ultrasound predicts treatment outcome in patients with Crohn's disease. Inflamm Bowel Dis. 2014;20(11):2029–37.
234. Li HH, Zhu H, Yue L, Fu Y, Grimm R, Stemmer A, et al. Feasibility of free-breathing dynamic contrast-enhanced MRI of gastric cancer using a golden-angle radial stack-of-stars VIBE sequence: comparison with the conventional contrast-enhanced breath-hold 3D VIBE sequence. Eur Radiol. 2018;28(5):1891–9.
235. Zhang A, Song J, Ma Z, Chen T. Combined dynamic contrast-enhanced magnetic resonance imaging and diffusion-weighted imaging to predict neoadjuvant chemotherapy effect in FIGO stage IB2-IIA2 cervical cancers. Radiol Med. 2020;125(12):1233–42.
236. De Piano F, Buscarino V, Maresca D, Maisonneuve P, Aletti G, Lazzari R, et al. Do DWI and quantitative DCE perfusion MR have a prognostic value in high-grade serous ovarian cancer? Radiol Med. 2019;124(12):1315–23.
237. Li HM, Qiang JW, Ma FH, Zhao SH. The value of dynamic contrast-enhanced MRI in characterizing complex ovarian tumors. J Ovarian Res. 2017;10(1):4.
238. Sala E, Rockall A, Rangarajan D, Kubik-Huch RA. The role of dynamic contrast-enhanced and diffusion weighted magnetic resonance imaging in the female pelvis. Eur J Radiol. 2010;76(3):367–85.
239. Du L, Li X, Qiu X, Liu X, Wang Y, Yu Y. Application of FLASH-3D dynamic contrast-enhanced imaging for diagnosis of endometrial carcinoma. Br J Radiol. 2016;89(1066):20160268.
240. Manfredi R, Mirk P, Maresca G, Margariti PA, Testa A, Zannoni GF, et al. Local-regional staging of endometrial carcinoma: role of MR imaging in surgical planning. Radiology. 2004;231(2):372–8.
241. Lin G, Huang YT, Chao A, Lin YC, Yang LY, Wu RC, et al. Endometrial cancer with cervical stromal invasion: diagnostic accuracy of diffusion-weighted and dynamic contrast enhanced MR imaging at 3T. Eur Radiol. 2017;27(5):1867–76.
242. Ippolito D, Minutolo O, Cadonici A, Talei Franzesi C, Bonaffini P, Perego P, et al. Endometrial cancer: diagnostic value of quantitative measurements of microvascular changes with DCE-MR imaging. MAGMA. 2014;27(6):531–8.
243. Jalaguier-Coudray A, Villard-Mahjoub R, Delouche A, Delarbre B, Lambaudie E, Houvenaeghel G, et al. Value of dynamic contrast-enhanced and diffusion-weighted MR imaging in the detection of pathologic complete response in cervical cancer

after neoadjuvant therapy: a retrospective observational study. Radiology. 2017;284(2):432–42.
244. Dappa E, Elger T, Hasenburg A, Duber C, Battista MJ, Hotker AM. The value of advanced MRI techniques in the assessment of cervical cancer: a review. Insights Imaging. 2017;8(5):471–81.
245. Zhang Z, Wang Z, Zhao R. Dynamic contrast-enhanced magnetic resonance imaging of advanced cervical carcinoma: the advantage of perfusion parameters from the peripheral region in predicting the early response to radiotherapy. Int J Gynecol Cancer. 2018;28(7):1342–9.
246. Ciolina M, Vinci V, Villani L, Gigli S, Saldari M, Panici PB, et al. Texture analysis versus conventional MRI prognostic factors in predicting tumor response to neoadjuvant chemotherapy in patients with locally advanced cancer of the uterine cervix. Radiol Med. 2019;124(10):955–64.
247. Albano D, Benenati M, Bruno A, Bruno F, Calandri M, Caruso D, et al. Imaging side effects and complications of chemotherapy and radiation therapy: a pictorial review from head to toe. Insights Imaging. 2021;12(1):76.
248. Messina C, Bignone R, Bruno A, Bruno A, Bruno F, Calandri M, et al. Diffusion-Weighted Imaging in Oncology: An Update. Cancers (Basel). 2020;12(6).
249. Hameeduddin A, Sahdev A. Diffusion-weighted imaging and dynamic contrast-enhanced MRI in assessing response and recurrent disease in gynaecological malignancies. Cancer Imaging. 2015;15:3.
250. Cosgrove D, Lassau N. Imaging of perfusion using ultrasound. Eur J Nucl Med Mol Imaging. 2010;37(Suppl 1):S65-85.
251. Hudson JM, Karshafian R, Burns PN. Quantification of flow using ultrasound and microbubbles: a disruption replenishment model based on physical principles. Ultrasound Med Biol. 2009;35(12):2007–20.
252. Lamuraglia M, Escudier B, Chami L, Schwartz B, Leclere J, Roche A, et al. To predict progression-free survival and overall survival in metastatic renal cancer treated with sorafenib: pilot study using dynamic contrast-enhanced Doppler ultrasound. Eur J Cancer. 2006;42(15):2472–9.
253. Notohamiprodjo M, Reiser MF, Sourbron SP. Diffusion and perfusion of the kidney. Eur J Radiol. 2010;76(3):337–47.
254. Braunagel M, Graser A, Reiser M, Notohamiprodjo M. The role of functional imaging in the era of targeted therapy of renal cell carcinoma. World J Urol. 2014;32(1):47–58.
255. Michaely HJ, Sourbron SP, Buettner C, Lodemann KP, Reiser MF, Schoenberg SO. Temporal constraints in renal perfusion imaging with a 2-compartment model. Invest Radiol. 2008;43(2):120–8.
256. Li SP, Padhani AR. Tumor response assessments with diffusion and perfusion MRI. J Magn Reson Imaging. 2012;35(4):745–63.
257. Hackstein N, Heckrodt J, Rau WS. Measurement of single-kidney glomerular filtration rate using a contrast-enhanced dynamic gradient-echo sequence and the Rutland-Patlak plot technique. J Magn Reson Imaging. 2003;18(6):714–25.
258. Michaely HJ, Schoenberg SO, Oesingmann N, Ittrich C, Buhlig C, Friedrich D, et al. Renal artery stenosis: functional assessment with dynamic MR perfusion measurements–feasibility study. Radiology. 2006;238(2):586–96.
259. Conlin CC, Huang Y, Gordon BAJ, Zhang JL. Quantitative characterization of glomerular fibrosis with magnetic resonance imaging: a feasibility study in a rat glomerulonephritis model. Am J Physiol Renal Physiol. 2018;314(5):F747–52.
260. Wentland AL, Sadowski EA, Djamali A, Grist TM, Becker BN, Fain SB. Quantitative MR measures of intrarenal perfusion in the assessment of transplanted kidneys: initial experience. Acad Radiol. 2009;16(9):1077–85.
261. Abdel Razek AA, Mousa A, Farouk A, Nabil N. Assessment of semiquantitative parameters of dynamic contrast-enhanced perfusion MR imaging in differentiation of subtypes of renal cell carcinoma. Pol J Radiol. 2016;81:90–4.
262. Scialpi M, Di Maggio A, Midiri M, Loperfido A, Angelelli G, Rotondo A. Small renal masses: assessment of lesion characterization and vascularity on dynamic contrast-enhanced MR imaging with fat suppression. AJR Am J Roentgenol. 2000;175(3):751–7.
263. Sun MR, Ngo L, Genega EM, Atkins MB, Finn ME, Rofsky NM, et al. Renal cell carcinoma: dynamic contrast-enhanced MR imaging for differentiation of tumor subtypes–correlation with pathologic findings. Radiology. 2009;250(3):793–802.
264. F Gentili I Bronico U Maestroni F Ziglioli EM Silini S Buti et al 2020 Small renal masses (</= 4 cm): differentiation of oncocytoma from renal clear cell carcinoma using ratio of lesion to cortex attenuation and aorta-lesion attenuation difference (ALAD) on contrast-enhanced CT Radiol Med 125 12 1280 7
265. Hahn OM, Yang C, Medved M, Karczmar G, Kistner E, Karrison T, et al. Dynamic contrast-enhanced magnetic resonance imaging pharmacodynamic biomarker study of sorafenib in metastatic renal carcinoma. J Clin Oncol. 2008;26(28):4572–8.
266. van der Pol CB, Chung A, Lim C, Gandhi N, Tu W, McInnes MDF, et al. Update on multiparametric MRI of urinary bladder cancer. J Magn Reson Imaging. 2018;48(4):882–96.
267. Rosenkrantz AB, Geppert C, Grimm R, Block TK, Glielmi C, Feng L, et al. Dynamic contrast-enhanced MRI of the prostate with high spatiotemporal resolution using compressed sensing, parallel imaging, and continuous golden-angle radial sampling: preliminary experience. J Magn Reson Imaging. 2015;41(5):1365–73.
268. Rabie E, Faeghi F, Izadpanahi MH, Dayani MA. Role of Dynamic Contrast-Enhanced Magnetic Resonance Imaging in Staging of Bladder Cancer. J Clin Diagn Res. 2016;10(4):TC01-5.
269. Zhou G, Chen X, Zhang J, Zhu J, Zong G, Wang Z. Contrast-enhanced dynamic and diffusion-weighted MR imaging at 3.0T to assess aggressiveness of bladder cancer. Eur J Radiol. 2014;83(11):2013-8.
270. Angileri SA, Di Meglio L, Petrillo M, Arrichiello A, Pandolfi M, Roda GM, et al. Software-assisted US/MRI fusion-targeted biopsy for prostate cancer. Acta Biomed. 2020;91(10-S):2020006.
271. Beyhan M, Sade R, Koc E, Adanur S, Kantarci M. The evaluation of prostate lesions with IVIM DWI and MR perfusion parameters at 3T MRI. Radiol Med. 2019;124(2):87–93.
272. Gundogdu E, Emekli E, Kebapci M. Evaluation of relationships between the final Gleason score, PI-RADS v2 score, ADC value, PSA level, and tumor diameter in patients that underwent radical prostatectomy due to prostate cancer. Radiol Med. 2020;125(9):827–37.
273. Abdollahi H, Mofid B, Shiri I, Razzaghdoust A, Saadipoor A, Mahdavi A, et al. Machine learning-based radiomic models to predict intensity-modulated radiation therapy response, Gleason score and stage in prostate cancer. Radiol Med. 2019;124(6):555–67.
274. Brunese L, Mercaldo F, Reginelli A, Santone A. Formal methods for prostate cancer Gleason score and treatment prediction using radiomic biomarkers. Magn Reson Imaging. 2020;66:165–75.
275. Weinreb JC, Barentsz JO, Choyke PL, Cornud F, Haider MA, Macura KJ, et al. PI-RADS Prostate Imaging - Reporting and Data System: 2015, Version 2. Eur Urol. 2016;69(1):16–40.
276. De Visschere PJ, Vral A, Perletti G, Pattyn E, Praet M, Magri V, et al. Multiparametric magnetic resonance imaging characteristics of normal, benign and malignant conditions in the prostate. Eur Radiol. 2017;27(5):2095–109.

277. Cybulski AJ, Catania M, Brancato S, Cogo N, di Paola V, Pozzi Mucelli R, et al. Added value of MRI tractography of peri-prostatic nerve plexus to conventional T2-WI in detection of extra-capsular extension of prostatic cancer. Radiol Med. 2019;124(10):946–54.
278. Turkbey B, Rosenkrantz AB, Haider MA, Padhani AR, Villeirs G, Macura KJ, et al. Prostate Imaging Reporting and Data System Version 2.1: 2019 Update of Prostate Imaging Reporting and Data System Version 2. Eur Urol. 2019;76(3):340-51.
279. Lovegrove CE, Matanhelia M, Randeva J, Eldred-Evans D, Tam H, Miah S, et al. Prostate imaging features that indicate benign or malignant pathology on biopsy. Transl Androl Urol. 2018;7(Suppl 4):S420–35.
280. Chatterjee A, Gallan AJ, He D, Fan X, Mustafi D, Yousuf A, et al. Revisiting quantitative multi-parametric MRI of benign prostatic hyperplasia and its differentiation from transition zone cancer. Abdom Radiol (NY). 2019;44(6):2233–43.
281. Patel P, Mathew MS, Trilisky I, Oto A. Multiparametric MR imaging of the prostate after treatment of prostate cancer. Radiographics. 2018;38(2):437–49.
282. Meier-Schroers M, Kukuk G, Wolter K, Decker G, Fischer S, Marx C, et al. Differentiation of prostatitis and prostate cancer using the Prostate Imaging-Reporting and Data System (PI-RADS). Eur J Radiol. 2016;85(7):1304–11.
283. Cutaia G, Tosto G, Cannella R, Bruno A, Leto C, Salvaggio L, et al. Prevalence and clinical significance of incidental findings on multiparametric prostate MRI. Radiol Med. 2020;125(2):204–13.
284. Coppola A, Platania G, Ticca C, De Mattia C, Bortolato B, Palazzi MF, et al. Sensitivity of CE-MRI in detecting local recurrence after radical prostatectomy. Radiol Med. 2020;125(7):683–90.
285. Mazaheri Y, Akin O, Hricak H. Dynamic contrast-enhanced magnetic resonance imaging of prostate cancer: A review of current methods and applications. World J Radiol. 2017;9(12):416–25.
286. Park SY, Park BK, Kwon GY. Diagnostic performance of mass enhancement on dynamic contrast-enhanced MRI for predicting clinically significant peripheral zone prostate cancer. AJR Am J Roentgenol. 2020;214(4):792–9.
287. Gurgitano M, Angileri SA, Roda GM, Liguori A, Pandolfi M, Ierardi AM, et al. Interventional Radiology ex-machina: impact of Artificial Intelligence on practice. Radiol Med. 2021;126(7):998–1006.
288. Kim SH, Choi MS, Kim MJ, Kim YH, Cho SH. Role of semiquantitative dynamic contrast-enhanced MR imaging in characterization and grading of prostate cancer. Eur J Radiol. 2017;94:154–9.
289. G Badalamenti C Messina I Luca De E Musso A Casarin L Incorvaia 2019 Soft tissue sarcomas in the precision medicine era: new advances in clinical practice and future perspectives Radiol Med 124 4 259 65
290. Carotti M, Salaffi F, Beci G, Giovagnoni A. The application of dual-energy computed tomography in the diagnosis of musculoskeletal disorders: a review of current concepts and applications. Radiol Med. 2019;124(11):1175–83.
291. Gentili F, Cantarini L, Fabbroni M, Nigri A, Mazzei FG, Frediani B, et al. Magnetic resonance imaging of the sacroiliac joints in SpA: with or without intravenous contrast media? A preliminary report. Radiol Med. 2019;124(11):1142–50.
292. Minutoli F, Pergolizzi S, Blandino A, Mormina E, Amato E, Gaeta M. Effect of granulocyte colony-stimulating factor on bone marrow: evaluation by intravoxel incoherent motion and dynamic contrast-enhanced magnetic resonance imaging. Radiol Med. 2020;125(3):280–7.
293. Ostergaard M, Boesen M. Imaging in rheumatoid arthritis: the role of magnetic resonance imaging and computed tomography. Radiol Med. 2019;124(11):1128–41.
294. Nascimento D, Suchard G, Hatem M, de Abreu A. The role of magnetic resonance imaging in the evaluation of bone tumours and tumour-like lesions. Insights Imaging. 2014;5(4):419–40.
295. Bellelli A, Silvestri E, Barile A, Albano D, Aliprandi A, Caudana R, et al. Position paper on magnetic resonance imaging protocols in the musculoskeletal system (excluding the spine) by the Italian College of Musculoskeletal Radiology. Radiol Med. 2019;124(6):522–38.
296. Drape JL. Advances in magnetic resonance imaging of musculoskeletal tumours. Orthop Traumatol Surg Res. 2013;99(1 Suppl):S115-23.
297. Bruno F, Arrigoni F, Mariani S, Splendiani A, Di Cesare E, Masciocchi C, et al. Advanced magnetic resonance imaging (MRI) of soft tissue tumors: techniques and applications. Radiol Med. 2019;124(4):243–52.
298. Costa FM, Canella C, Gasparetto E. Advanced magnetic resonance imaging techniques in the evaluation of musculoskeletal tumors. Radiol Clin North Am. 2011;49(6):1325-58, vii-viii.
299. V Chianca D Albano C Messina G Vincenzo S Rizzo F Grande Del et al 2021 An update in musculoskeletal tumors: from quantitative imaging to radiomics Radiol Med 126 8 1095 105
300. Robba T, Chianca V, Albano D, Clementi V, Piana R, Linari A, et al. Diffusion-weighted imaging for the cellularity assessment and matrix characterization of soft tissue tumour. Radiol Med. 2017;122(11):871–9.
301. Hong SH, Choi JY, Lee JW, Kim NR, Choi JA, Kang HS. MR imaging assessment of the spine: infection or an imitation? Radiographics. 2009;29(2):599–612.